ISSN 0915-633X

# NATIONAL INSTITUTE FOR FUSION SCIENCE

## Ignition Characteristics in D-T Helical Reactors

O. Mitarai and S. Sudo

(Received - Aug.6, 1993 )

NIFS-283 June 1994

RESEARCH REPORT
NIFS Series



NAGOYA, JAPAN

# Ignition Characteristics in D-T Helical Reactors

O. MITARAI

Department of Electrical Engineering,

Kumamoto Institute of Technology,

Ikeda 4-22-1, Kumamoto 860 Japan

S. SUDO

National Institute for Fusion Science,

Chikusa-ku, Furo-cho, Nagoya, 464-01 Japan

## Abstract

Ignition characteristics in D-T helical reactors of various sizes are studied with the operation path method on the $\bar{P}_{ht}\tau_E^2$-T plane and the POPCON method. Based on the empirical LHD scaling, a confinement has to be improved by more than a factor of 1.5 for reaching ignition and more than a factor $\gamma_H = 2$ to have optimum fusion power in a reference helical reactor with $R > 8$ m, $\bar{a} = 2$ m, and $B_0 > 6$ T. The density limit and the confinement time saturation effect with respect to the density degrade the favorable density scaling of the confinement time ($\tau_E \propto n^{0.69}$) and are found to be important limiting factors for ignition characteristics. For a reactor of $R = 10$ m, $\bar{a} = 2$ m, $\gamma_H = 2$, $B_0 = 7$ T with an external heating power $P_{ex} = 100$ MW, the minimum auxiliary heating power is around 55 MW at an operating density 40 % below the density limit, and ignition can be reached in a finite time. The ignition characteristics for larger size ($R = 15$ and 20 m) reactors and gyro-reduced Bohm scaling are also studied.

---

**Key Words:** Ignition Characteristics, D-T Helical Reactor, Density Limit

## 1. Introduction

A helical reactor can operate in steady state without a large recirculation power if the bootstrap current can be canceled by a small non-inductive current drive power or if it can be utilized for confinement improvement and no large amount of power is needed to induce the electric field. This is an advantage in a helical reactor compared with a tokamak, which needs a large recirculation power of around 100 MW[1] for non-inductive current drive to obtain steady state operation. Although this disadvantage in a tokamak can be removed by employing an inductive alternating current (AC) operation with efficient use of an Ohmic transformer,[2] the power supply for the Ohmic transformer has to include a superconducting magnetic energy storage (SMES) unit, which, however, because of its efficiency, needs only a small amount of power. In a helical reactor, both the requirement of a large recirculation power and a SMES unit can potentially be removed, leading to a simpler machine with small power supply units. We thus have an incentive to study a helical reactor.

While ignition characteristics in a tokamak reactor have actively been studied by many groups,[3]-[6] those in the helical reactor have not received much attention.[7]-[10] This might be due to the lack so far of the established confinement scaling. The LHD scaling proposed by Sudo et al.[11] and the gyro-reduced Bohm (GRB) scaling[12] are gaining acceptance in helical experiments.[13] Using methods developed in ignition studies for a tokamak reactor, such as the operation path method on $n\tau_E$-T and $\overline{P}_{ht}\tau_E^2$-T planes[14]-[17] and "POPCON"[18], we are now able to study the ignition characteristics of a helical reactor based on the empirical scaling law.

Using LHD scaling, a study of the helical reactor had been made on POPCON.[19] However, the density limit, which is very important as will be seen in this study, was not taken into account. The confinement time saturation effect with respect to density recently observed,[20] which can alter the ignition characteristics, had not been considered yet.

In this paper, we present the ignition characteristics in various sizes of helical

reactors using the operation path method, and estimate the auxiliary heating power to reach ignition using the POPCON method. A confinement enhancement factor of 1.5 is required to reach ignition for LHD and GRB scalings; however, a factor of 2 or more must be realized for optimum fusion power (~ 3 to 3.5 GW) at the operation point on the ignition boundary. For example, we have also found that the density limit is a limiting factor for reducing the auxiliary heating power and for having optimum fusion power, and the confinement time saturation effect can alter the ignition characteristics. This is due to the fact that the point of minimum heating power exists above or around the density limit in many cases and the confinement time saturation effect increases the plasma conduction loss. Ignition capabilities of various sizes of helical reactors are also presented.

In section 2, we describe the formula for operation paths for the LHD and GRB scalings and the ignition boundaries on the $\overline{P}_{ht}\tau_E^2$-T plane. In section 3, the confinement enhancement factors required for reaching ignition are obtained using the operation path method for the proposed helical reactors. In section 4, we evaluate the auxiliary heating power and operating point of helical reactors using the POPCON method including the density limit and the confinement time saturation effect with respect to the density. In section 5 and 6, a discussion and summary are presented, respectively.

## 2. Operation Path for the LHD and GRB Scalings and Ignition boundary

Since a helical reactor has no Ohmic heating power, and hence no Ohmic heating confinement time such as that described by neo-Alcator scaling in a tokamak, the ignition analyses are relatively simpler than a tokamak reactor. In this study, we use two scalings, LHD and GRB. The operation path on the ignition boundary can provide the confinement enhancement factor required for reaching ignition in various reactors without knowing the detailed heating power input. Therefore it is convenient to use this method to know the overall behavior of a reactor and to compare the performance in various reactors.

### (2.1) Operation Path Parameter for the LHD Scaling

We employ the LHD scaling proposed by Sudo et al.,[11] which has been confirmed in many helical experiments and is gaining acceptance.[12][13] The LHD scaling with a confinement enhancement factor $\gamma_H$ is given by[11]

$$\tau_{E,LHD}\,[s] = \gamma_H\, 0.17\, \bar{n}_{20}^{0.69}\, \left[\times 10^{20}\,m^{-3}\right] B_o^{0.84}\,[T]\, \bar{a}^{2.0}[m]\, R^{0.75}\,[m] / P_H^{0.58}\,[MW] \quad . (2\text{-}1)$$

where $\bar{a}$ is the average minor radius. For the reference reactor with R = 10 m, $\bar{a}$ = 2m, $B_o$= 7 T, $\bar{n}_{20} = 2\times10^{20}\ m^{-3}$, the confinement time is 4.37 sec for $\gamma_H = 2$ and $P_H$ = 100 MW. In this study. we further take into account the confinement time saturation effect with respect to the operating density as follows;[20]

$$\begin{cases} (1)\ \bar{n} \le \bar{n}_{SH} & : \quad \tau_E = \tau_{E,LHD}(\bar{n}) \qquad (2\text{-}2) \\ (2)\ \bar{n}_{SH} \le \bar{n} \le \bar{n}_{lim} & : \quad \tau_E = \tau_{E,LHD}(\bar{n}_{SH}) \qquad (2\text{-}3) \end{cases}$$

where the confinement saturation density $\bar{n}_{SH}$ is given by $\bar{n}_{SH} = \gamma_S\, \bar{n}_{lim}$ with $\gamma_S$ = 0.6 in this study,[10] and the line-averaged density limit is given by[8]

$$\bar{n}_{lim}[m^{-3}] = 0.25 \times 10^{20} \sqrt{P_H[MW]\, B_o[T] / \bar{a}^2[m]\, R[m]} \quad . \qquad (2\text{-}4)$$

Replacing the total heating power $P_H$ in Eq. (2-1) with $P_H = \bar{P}_{ht,net}\, 2\pi R \pi\, \bar{a}^2$, namely $\bar{P}_{ht,net}$ the net heating power density times the plasma volume, we have the confinement formula as $\tau_E = \gamma_H C_{op} / (\bar{P}_{ht,net})^{0.58}$ with the coefficient:

$$C_{op}^2(\bar{n})\left[(MW/m^3 \cdot s^2)^{1.16}\right] = 9.085 \times 10^{-4}\, \bar{n}_{20}^{1.38}\left[\times 10^{20}\, m^{-3}\right] B_o^{1.68}[T]\, \bar{a}^{1.68}[m]\, R^{0.34}[m] \,, \qquad (2\text{-}5)$$

which is called "the operation path parameter" and reveals the ignition capability of a fusion reactor. The values of the operation path parameter $C_{op}^2$ are listed in Table 1 for various sizes of proposed, Helical Reactors (HELICAR) with a low aspect ratio (-LA) such as the compact torsatron type reactor with a major radius of 8 and 10 m,[8]-[10] as well as high aspect ratio (-HA) devices such as the conventional type reactor with R of 15 to 20 m, and the Heliotron reactor.[7]

**(2.2) Operation Path Parameter**

The gyro-reduced Bohm (GRB) scaling has recently been proposed based on the trapped particle drift wave theory except for the ion mass correction and plasma elongation.[12] This scaling provides a slightly smaller confinement time than the LHD scaling for the same machine. The GRB scaling with a confinement enhancement factor $\gamma_H$ is given by[12]

$$\tau_E\,[s] = \gamma_H\, 0.25\, \bar{n}_{20}^{0.6}\left[\times 10^{20}\, m^{-3}\right] B_o^{0.8}[T]\, a^{2.4}[m]\, R^{0.6}[m]\, \kappa\, A_i^{-0.2} / P_H^{0.6}\,[MW] \,. \qquad (2\text{-}6)$$

where $A_i$ is the average mass factor (= 2.5 for D-T plasma), $\kappa$ is the plasma elongation, and a is the plasma minor radius. For the reference reactor with R =10 m, $B_o = 7$ T, $\bar{n}_{20} = 1 \times 10^{20}\, m^{-3}$, $\gamma_H = 1$ and $P_H = 100$ MW, the confinement time is 1.53 sec for a = $\sqrt{2}$ m

and $\kappa = 2$, and $\tau_E = 1.76$ sec for a = 2 m and $\kappa = 1$, which are both smaller than the LHD confinement time $\tau_E = 1.92$ sec. Here, the plasma cross section (and hence the plasma volume) is taken to be the same for both scalings, and therefore the relation $\bar{a}^2 = a^2\kappa$ is used. However we have used $\kappa = 1$ throughout this work.

The operation path parameter for GRB scaling is given by $\tau_E = \gamma_H C_{op} / (\bar{P}_{ht,net})^{0.6}$ and $P_H = \bar{P}_{ht,net}\, 2\pi R \pi a^2 \kappa$ as

$$C_{op}{}^2(\bar{n})\left[(MW/m^3{\cdot}s^2)^{1.2}\right] = 1.760\times10^{-3}\,\bar{n}_{20}{}^{1.2}\left[\times10^{20}\ m^{-3}\right] B_o{}^{1.6}[T]\, a^{2.4}[m] \times \kappa^{0.8}\, A_i{}^{-0.4} \quad . \tag{2-7}$$

It is interesting to note that as the operation path parameter $C_{op}{}^2$ for GRB scaling is independent of the plasma major radius R, as is also seen in Table 1, the ignition capability of reference reactors with the same minor radius are all the same. We also notice that the operation path parameter for GRB scaling is always lower than that for LHD scaling for the case $\kappa \geq 1$ and hence $\bar{a} \geq a$. If the negative dependence of the mass effect can be removed from GRB scaling, the operation path parameters are both comparable for $\kappa = 1$ and $\bar{a} = a$.

### (2.3) Ignition Boundary

The ignition boundaries on the $n\tau_E$-T and $\bar{P}_{h\,t}\tau_E{}^2$-T planes can be obtained from the generalized global power balance equation in steady state[14)-17)] derived from $\dot{W} = \bar{P}_{ht} - \{\bar{P}_L - (\bar{P}_\alpha - \bar{P}_b)\}$ and $\dot{W} = 0$ as

$$\left[\bar{P}_{ht}\tau_E{}^2\right] = A_L\{n(0)\tau_E\} - (A_\alpha - A_b)\{n(0)\tau_E\}^2 \tag{2-8}$$

$$= -(A_\alpha - A_b)\left[n(0)\tau_E - \frac{A_L}{2(A_\alpha - A_b)}\right]^2 + \frac{A_L{}^2}{4(A_\alpha - A_b)}, \tag{2-9}$$

where $\dot{W}$ is the time derivative of the plasma energy, $\bar{P}_{ht}$ is the "auxiliary heating power density", $\bar{P}_L$ is the plasma conduction loss $\bar{P}_L = A_L n(0)/\tau_E$, $\bar{P}_\alpha$ is the alpha heating power density $\bar{P}_\alpha = A_\alpha n(0)^2$, $\bar{P}_b$ is the bremsstrahlung loss $\bar{P}_b = A_b n(0)^2$, and the coefficients $A_L$, $A_\alpha$ and $A_b$ are given in the Appendix. We note that the synchrotron radiation loss is not taken into account in this study for simplicity. The well known ignition boundary on the $n\tau_E$-T plane is given by Eq. (2-8) as $\{n(0)\tau_E\}_{ig} = A_L/(A_\alpha - A_b)$. Another useful and convenient ignition boundary is obtained on the $\bar{P}_{ht}\tau_E^2$-T plane from the second term in Eq. (2-9) as [14]-[17]

$$[\bar{P}_{ht}\tau_E^2]_{ig} = \left\{ \frac{A_L^2}{4\,(A_\alpha - A_b)} \right\} = \frac{1}{4} \cdot A_L \{n(0)\tau_E\}_{ig} \qquad (2\text{-}10)$$

Its minimum value yields the saddle point described by $[\bar{P}_{ht}\tau_E^2]_{SDL}$, which provides the simple ignition criterion for the power law scaling $\tau_E \propto \bar{P}_{ht}^{-S}$ and $S = 0.5$. As S is larger than 0.5 for LHD and GRB scalings in this study, the saddle point given here is less meaningful. The whole ignition boundary should be drawn, and if the ignition boundary is lower than the height of the operation path given below, the reactor can be in the ignition regime.

**(2.4) Operation Path**

For the generalized expression of the confinement time $\tau_E = \gamma_H C_{op}/(\bar{P}_{ht,net})^S$, the resultant confinement time and the operation path can be given, with the help of the power balance equation $\bar{P}_{ht,net} = \bar{P}_{ht} - \dot{W} + \bar{P}_\alpha - \bar{P}_b = \bar{P}_L = n(0)A_L x 10^{-6}/\tau_E$ [MW/m$^3$], by [16][17]

$$\tau_E(n)[s] = \left[ \frac{\{\gamma_H^2 C_{op}(n)^2\}^{0.5/(1-S)}}{\{n(0)A_L \times 10^{-6}\}^{S/(1-S)}} \right], \qquad (2\text{-}11)$$

$$\{n(0)\tau_E\}_{op}[m^{-3}s] = n(0)\left[\frac{\{\gamma_H{}^2 C_{op}(n)^2\}^{0.5/(1-S)}}{\{n(0)A_L\times 10^{-6}\}^{S/(1-S)}}\right] . \qquad (2\text{-}12)$$

The height of the operation path is hence given by

$$\left[\bar{P}_{ht}\tau_E{}^2\right]_{op}[W/m^3\cdot s^2] = \frac{1}{4}\{n(0)A_L\}\left[\frac{\{\gamma_H{}^2 C_{op}(n)^2\}^{0.5/(1-S)}}{\{n(0)A_L\times 10^{-6}\}^{S/(1-S)}}\right]. \qquad (2\text{-}13)$$

The height of the operation path is constant with temperature for S = 0.5, decreases for S > 0.5, and increases for S < 0.5 as obtained in the previous study.[17]

### (2.5) Auxiliary Heating Power

The auxiliary heating power density for the "POPCON" analysis is calculated by ($\dot{W} = 0$)

$$\bar{P}_{ht}\,[W/m^3] = \bar{P}_L - (\bar{P}_\alpha - \bar{P}_b) \qquad (2\text{-}14)$$

where

$$\bar{P}_L(n)[W/m^3] = \frac{n(0)A_L}{\tau_E(n)} = n(0)A_L\left[\frac{\{n(0)A_L\times 10^{-6}\}^{S/(1-S)}}{\{\gamma_H{}^2 C_{op}(n)^2\}^{0.5/(1-S)}}\right]. \qquad (2\text{-}15)$$

The total auxiliary heating power calculated by $P_{HT} = \bar{P}_{ht}\,2\pi^2 R\bar{a}^2$ is described by the contour lines on the n-T plane.

### (2.6) Density Limit in the $\bar{P}_{ht}\tau_E{}^2$-T Plane

Using $P_H[MW] = \{n(0)A_L x 10^{-6}/\tau_E\}\,2\pi^2 R\bar{a}^2$ and the density profile parameter $\gamma_{pr} = n(0)_{lim}/\bar{n}_{lim}$ in Eq. (2-4), we have the density limit for the net heating power in the ignition regime ($P_{HT} = 0$) on the $n\tau_E$-T and $\bar{P}_{ht}\tau_E{}^2$-T plane, respectively

$$\{n(0)\tau_E\}_{lim}\ [m^{-3}s] = \gamma_{pr}^2\ 1.234\times10^{34} A_L B_o[T]\ , \tag{2-16}$$

$$\left[\bar{P}_{ht}\tau_E^2\right]_{lim}\ [W/m^3\cdot s^2] = \frac{1}{4} A_L \{n(0)\tau_E\}_{lim}\ . \tag{2-17}$$

The confinement saturation effect is not taken into account in this formula. The profile parameters are $\gamma_{pr} = 3/2, 15/8$ and $4/\pi$ for the parabolic density profile $\alpha_n = 1$, the peaked profile $\alpha_n = 2$ and the square root profile $\alpha_n = 0.5$, respectively. Since the density limit scaling is originally given for the average value, it becomes lower for the peaked profile, and higher for the flat profile, as is determined by the $\gamma_{pr}$ and $\alpha_n$ values. We have used the parabolic density profile throughout this paper unless otherwise noted. Density limit lines given by Eq. (2-17) in the ignition regime are drawn on the $\bar{P}_{ht}\tau_E^2$-T plane by the hatched line as will be seen in Figs.2 and 3.

### (2.7) Density Limit on POPCON

The density limit on POPCON is determined by the sum of the net heating power density ( = the plasma conduction loss $\bar{P}_L$ (Eq. 2-15)) and the external auxiliary heating power $P_{ex}$, as

$$n(0)_{lim}\ [m^{-3}] = \gamma_{pr}\ 0.25\times10^{20}\ \sqrt{\{2\pi^2\bar{P}_L(n(0)) + P_{ex}/(\bar{a}^2 R)\}B_o[T]}\ . \tag{2-18}$$

It is to be noted here that an external heating power $P_{ex}$ larger than $P_{HT}$ should be applied to reach ignition within a finite time with positive $\dot{W}$, and to open the density window. In the ignition regime, $P_{ex}$ can be zero and therefore the density limit becomes lower.

#### (2.7.1) Confinement Time Saturation Effect and Density Limit During Heating Phase

When we take into account the confinement time saturation effect in the density regime $n(0)_{SH} \le n(0) \le n(0)_{lim}$, the density limit itself in the heating phase ($P_{ex} > P_{HT} > 0$) can be numerically determined by Eq. (2-18) inserting the plasma conduction

loss given by $\tau_E(n_{SH})$:

$$\bar{P}_L(n_{lim})\ [MW/m^3] = \frac{n(0)_{lim}A_L\times10^{-6}}{\tau_E(n_{SH})} = n(0)_{lim}A_L\times10^{-6}\left[\frac{\{n_{SH}(0)A_L\times10^{-6}\}^{S/(1-S)}}{\{\gamma_H^2 C_{op}(n_{SH}(0))^2\}^{0.5/(1-S)}}\right], \quad (2\text{-}19)$$

and $n_{SH}(0) = \gamma_S n(0)_{lim}$. The right hand side of Eq. (2-18) is drawn in Fig. 1 as indicated by "Density Limit Scaling" and the left-hand side is drawn as $n_{lim}(0)$ in Fig. 1. This intersection point provides the density limit, $n_{lim}(0)$.

The confinement time calculated from Eq. (2-11) is plotted for LHD scaling in Fig. 1, together with $\bar{P}_L$ and $n(0)_{lim}$ for the case of the reference reactor R = 10 m, $\bar{a} = 2$ m, $B_o = 7$ T, $\gamma_H = 2$, T(0) = 10 keV and $\alpha_n = 1$. The case for $\gamma_S = 0.6$ is shown by the solid line, and for $\gamma_S = 1.0$ by the dotted line. For the density regime of $n(0)_{SH} \le n(0) \le n(0)_{lim}$, it is seen that the confinement time is saturated with respect to the density, the plasma conduction loss $\bar{P}_L$ calculated by $\bar{P}_L[MW/m^3] = n(0)A_L\,x10^{-6}/\tau_E(n_{SH})$ increases linearly with the density and is larger than that for $\gamma_S = 1$. Therefore the density limit increases slightly from $1.85x10^{20}\ m^{-3}$ (Point A) to $1.9x10^{20}\ m^{-3}$ (Point B) compared to the case without the confinement time saturation effect as seen in Fig. 1.

We should note that the confinement time calculated from Eq. (2-11) is independent of the electron density for GRB scaling with the power factor S = 0.6 and $C_{op}^2 \propto n(0)^2$ (Eq. (2-7)). Therefore the confinement time saturation effect does not appear in POPCON as will be seen in Fig. 8.

**(2.7.2) Density Limit in the Ignition Regime**

The density limit for any profile in the ignition regime ($P_{HT} = 0, P_{ex} = 0$ and $\bar{P}_{ht,net} = \bar{P}_L > 0$) can be simply obtained, for example in the case of the LHD scaling, as

$$n(0)_{lim}\ [m^{-3}] = 10^{20}\left[\frac{1.2337\,\gamma_{pr}^2 B_o \{A_L\times10^{14}\}^{1/(1-S)}}{\{\gamma_H^2 D_{op}^2/\gamma_{pr}^{1.38}\}^{0.5/(1-S)}\,\gamma_S^{(0.69-S)/(1-S)}}\right]^{\frac{1-S}{1.69-2S}}, \quad (2\text{-}20)$$

where $D_{op}^2 = C_{op}^2/\bar{n}_{20}^{1.38}$ is given by Eq. (2-5). When $\gamma_S$ approaches unity, the density limit becomes the one without the confinement time saturation effect. We also see from Eq. (2-20) that the density limit is lowered for the higher confinement enhancement factor $\gamma_H$ because the plasma conduction loss and hence the net heating power decrease.

## 3. Operation Path Method for Ignition Criterion

With LHD scaling, similar to the L-mode in a tokamak, it is necessary to improve the confinement to some extent for reaching ignition in the various proposed helical reactors. As done in the tokamak reactor design, we will estimate the confinement enhancement factor $\gamma_H$ required for reaching ignition using the operation path method.[17] In this study, we consider various sizes of helical reactors, which are divided into two groups,these are conventional high aspect ratio (A > 7), HELICAR-HA, and the low aspect ratio (A < 5) helical reactors, HELICAR-LA, as listed in Table 1.

The operation paths on the $\bar{P}_{ht}\tau_E^2$-T plane for various densities are shown in Fig. 2 for the reference helical reactor R = 10 m, $\bar{a}$ = 2 m, and $B_0$ = 7 T. The following plasma parameters are assumed throughout the paper unless otherwise noted: the density and temperature profiles corresponding to $\alpha_n = \alpha_T = 1$, the ion to electron temperature ratio $T_i(0)/T_e(0) = 1$, the effective ion charge $Z_{eff} = 1.5$, the alpha particle density fraction to the electron density $f_\alpha = 0.05$, the average impurity charge Z = 7 and the deuterium and tritium fuel density fraction to the electron density $f_D = f_T = 0.415$. The ignition boundaries for various alpha confinement fractions $\eta_\alpha$ = 0.7 to 1.0 are drawn in Fig.2. As the alpha particle confinement is improved, the ignition boundary expands and the saddle point corresponding to the minimum point on the $[\bar{P}_{ht}\tau_E^2]_{ig}$ line becomes lower. In this study we employ the low $\eta_\alpha$ = 0.7 value as expected in the compact torsatron reactor design.[19] The operation paths are indicated by the solid lines corresponding to LHD scaling with $\gamma_H$ = 2, by dot-dashed lines to GRB scaling with $\gamma_H$ = 2, and by the dashed lines to LHD scaling with $\gamma_H$ = 1.5, and by the dotted lines to the

GRB scaling with $\gamma_H = 1.5$. Since LHD scaling has the power law dependence $\tau_E \propto \bar{P}_{ht}^{-0.58}$, the operation path decreases with the temperature. This fact can be inferred from the previous study[17] such that in the case of $\tau_E \propto \bar{P}_{ht}^{-S}$ the operation path increases with the temperature for $S < 0.5$ and is constant (horizontal) for $S = 0.5$. In Fig. 2, the critical densities $n(0)_{ig}$ to reach ignition with LHD scaling can be obtained as ~ $2.4\times10^{20}$ m$^{-3}$ for $\gamma_H = 2$ and ~ $4.2\times10^{20}$ m$^{-3}$ for $\gamma_H = 1.5$. For GRB scaling, $n(0)_{ig}$ is ~ $3.0\times10^{20}$ m$^{-3}$ for $\gamma_H = 2$, and ~ $6.3\times10^{20}$ m$^{-3}$ for $\gamma_H = 1.5$, respectively. The hatched lines in the ignition regime indicate the density limit given by Eq.(2-17) and (2-16).

Fig. 3-(a) shows the operation paths for the various sizes of the helical reactor with $\bar{a} = 2$ m, $B_0 = 7$ T, and $\gamma_H = 2$ listed in Table 1 and the ignition boundaries for $\eta_\alpha = 0.7$ and LHD and GRB scalings with the fixed line-averaged density $\bar{n} = 2\times10^{20}$ m$^{-3}$. In the case of the parabolic density profile $\alpha_n = 1$, all the reactors can be in the ignition regime for LHD scaling and are marginal for GRB scaling. For a broader density profile, $\alpha_n = 0.5$, it becomes difficult to be in the ignition regime and the R = 8 m reactor cannot be in the ignition regime with this density. The density limit shown by the hatched line is slightly higher for the case of a flat density profile ($\alpha_n = 0.5$) than that of a parabolic profile ($\alpha_n = 1$).

For the case $\bar{a} = 2$ m, $B_0 = 6$ T, $\gamma_H = 2$, $\alpha_n = 1$ and $\bar{n} = 2\times10^{20}$ m$^{-3}$ as shown in Fig. 3-(b), reactors larger than R ~ 11 m can be in the ignition regime for LHD scaling, but all reactors are out of the ignition regime for GRB scaling. In this figure the operation path of the Heliotron (machine parameters are listed in Table 1) with $B_0 = 4$ T and $\gamma_H = 2$ is also shown using LHD scaling. For $\alpha_n = 1$ and $\bar{n} = 2\times10^{20}$ m$^{-3}$, the confinement must be improved up to $\gamma_H = 2.76$ to reach ignition in Heliotron with $B_0 = 4$ T, or the magnetic field has to be increased up to $B_0$ ~ 5.9 T with $\gamma_H = 2$.

For the case $\bar{a} = 2$ m, $B_0 = 8$ T, $\gamma_H = 1.5$, $\alpha_n = 1$ and $\bar{n} = 2\times10^{20}$ m$^{-3}$ as shown in Fig. 3-(c), reactors larger than R = 15 m can reach ignition for LHD scaling, but none of the reactors reach ignition for GRB scaling. We should note that in this calculation the line-averaged density is fixed at $\bar{n} = 2\times10^{20}$ m$^{-3}$, but if we increase the density, reaching

ignition is possible even in a smaller reactor and for GRB scaling as inferred from Fig. 2.

## 4. POPCON Analyses for Auxiliary Heating Power and Operating Point

To estimate the auxiliary heating power required for reaching ignition in proposed helical reactors, the POPCON method has been applied. This method is especially important in the helical reactor design, because the density limit and its effect on ignition can be clearly presented; for example the relative position of the Cordey pass at the minimum heating power to the density limit and the confinement time saturation effect with respect to the density can be well represented.

### (4.1) R = 10 m reactor

POPCON analyses are shown in Fig. 4-(a) and (b) for R = 10 m, $\bar{a}$ = 2 m, $B_o$ = 7 T, and $\gamma_H$ = 2 with and without the confinement saturation effect in terms of the density, respectively. The external heating power $P_{ex}$ = 100 MW is always applied to open the density window, namely to increase the density limit $n_{lim}(0)$ up to $1.6 \times 10^{20}$ $m^{-3}$ as shown by the hatched line. In Fig. 4-(a), the confinement time saturation regime between the density limit $n_{lim}(0)$ and the saturation density $n_{SH}(0) = 0.6\, n_{lim}(0)$ indicated by the dotted line is shown, where the plasma conduction loss increases and therefore the auxiliary heating power is increased, leading to the protrusion of the contour line compared to Fig. 4-(b). In the ignition regime, the external heating power can be reduced to zero, $P_{ex}$ = 0 MW, and then the density limit $n_{lim}(0)$ is lowered and the ignition boundary slightly shifts upward due to the larger plasma conduction loss in the confinement time saturation regime as shown in the figure. As the contour line with $P_{HT}$ = 100 MW, as shown by the dash-dot line, exists far below the density limit and its maximum heating power along the assumed operating density path $n_{SH}(0) = 0.6\, n_{lim}(0)$ is 55 MW, it can reach ignition in a finite time because the time derivative of the plasma energy $\dot{W}$ is positive for the externally applied $P_{ex}$ = 100 MW ( > $P_{HT}$ = 55

MW). We have also shown the volume average beta value $<\beta>$ with respect to the magnetic field strength by the long dashed lines. We should note that the pressure due to fusion alpha particles is not included in this beta value definition for simplicity. In fact, the beta contribution due to the fast alpha particle relative to the thermal beta is small as estimated in the following. While this is given by the analytical formula $\beta_\alpha/\beta_{th} \propto P_F\tau_s/(nT) \propto T^{5/2}$, which is obtained by the fusion rate $P_F \propto n^2T^2$ ($<\sigma v> \propto T^2$) and the slowing down time $\tau_s \propto T^{3/2}/n$, we have used the simpler empirical fit $\beta_\alpha/\beta_{th} = 0.29\,(f_D + f_T)^2(<T>[keV]/10 - 0.37)$ for $<T> \sim 7$ to 20 keV.[21] We obtain the small beta contribution as $\beta_\alpha = 0.125\,\beta_{th} = 0.05$ % for the representative parameters employed in this paper: $f_D = f_T = 0.415$, $<T> \sim 10$ keV, and $\beta_{th} \sim 4$ %.

It is also found that the contour line is discontinuous on both sides of the density limit line in Fig. 4-(a), which is different from Fig. 4-(b) without the confinement time saturation effect. We have also noticed that the Cordey pass, the minimum heating power point, is above the density limit, therefore it is very important to take into account the density limit and confinement time saturation effect with respect to the density for analyzing the ignition performance in a helical reactor. We have also seen that operation at the higher density and lower temperature is impossible in the helical reactor with LHD scaling as long as the density limit scaling in Eq. (2-4) holds.

The operating point (A) at $T_i(0) \sim 21$ keV, $n(0) \sim 2.9\times10^{20}$ m$^{-3}$, and $<\beta> \sim 3.0$ % on the ignition boundary ($P_{HT} = 0$ MW) in Fig. 4-(a) has the fusion power $P_f = (\bar{P}_\alpha + \bar{P}_n)2\pi^2R\bar{a}^2 \sim 3.0$ GW (the sum of the alpha particle heating power density $\bar{P}_\alpha$ including $\eta_\alpha = 0.7$ and 12.7 MeV neutron power density $\bar{P}_n$). The neutron wall loading at the operating point is 3.0 MW/m$^2$, which is calculated by the simple formula $W_n = \bar{P}_n 2\pi^2R\bar{a}^2/S$ with S being the average surface area of the vacuum chamber given by $S = (2\pi)^2Ra_w$ and $a_w = \bar{a} + 0.1$ (m). It is to be noted that although the helical system has a complex shape of vacuum chamber, we are just using the simplest formula for the plasma volume and surface. If the operating density is slightly increased up to $3.0\times10^{20}$ m$^{-3}$, the ion and electron temperatures are increased due to the thermonuclear instability

to around 25 keV as indicated by point (C) with $<\beta> \sim 3.7$ %, where somewhat larger fusion power $P_f \sim 4$ GW and the neutron wall loading $W_n \sim 4.2$ MW/m$^2$ are obtained. This indicates that a small change in the operating density leads to a large change in the fusion power and neutron wall loading. Therefore accurate control of the plasma parameters is of crucial importance in a reactor operation. For the case without a confinement time saturation effect, the ignition regime is somewhat widened, and hence the operating point (A) having a fusion power of $P_f \sim 3.0$ GW at $T_i(0) \sim 22.7$ keV, $n(0) \sim 2.74 \times 10^{20}$ m$^{-3}$, and $<\beta> \sim 3.1$ % is slightly removed from the density limit line as shown in Fig. 4-(b).

When the magnetic field strength is decreased to $B_o = 6$ T in the same reactor with $R = 10$ m, $\bar{a} = 2$ m and $\gamma_H = 2$, the ignition regime shifts upward mainly to the higher density regime as shown in Fig. 5-(a) because the height of the operation path is lowered. We have seen that the Cordey pass exists at a position much higher than the density limit line. In this ignition regime, the fusion power output is greater than 6 GW, and the average beta value is also larger than 6 %, which are both larger than the acceptable values for a helical reactor. If we increase the magnetic field strength up to $B_o = 8$ T, we can decrease the confinement enhancement factor. In Fig. 5-(b), the case for $\gamma_H = 1.5$ is shown for the same plasma parameters. The ignition regime shifts upward to the higher density regime similar to Fig. 5-(a) and the large fusion power of 5 GW is produced, but the beta value is to that in $<\beta> \geq 3\%$ due to the larger magnetic field. To have a similar performance with Fig. 4-(a), the confinement enhancement factor should be $\gamma_H = 1.8$.

**(4.2) R = 20 m reactor**

For a larger helical reactor $R = 20$ m, $\bar{a} = 2$ m, $B_o = 7$ T, and $\gamma_H = 2$, the operation path is higher, and hence the ignition regime is slightly widened as shown in POPCON in Fig. 6-(a). The density limit, however, becomes lower due to the lower heating power density. The operating point (C), with the somewhat large fusion power $P_f \sim 4$

GW and the smaller neutron wall loading, $W_n \sim 2.0$ MW/m$^2$, than that for the 10 m reactor, is around $T_i(0) \sim 22$ keV, $n(0) \sim 2.3 \times 10^{20}$ m$^{-3}$, and $\langle\beta\rangle \sim 2.5$ %. The operating point with $P_f \sim 3$ GW cannot be obtained in this case due to the large plasma volume.

If the confinement enhancement factor can be slightly increased up to $\gamma_H = 2.25$ as shown in Fig. 6-(b), the operating point (A) can have a fusion power ~ 3.0 GW and neutron wall loading ~ 1.5 MW/m$^2$ at $T_i(0) \sim 23.5$ keV, $n(0) \sim 1.9 \times 10^{20}$ m$^{-3}$, and $\langle\beta\rangle \sim$ 2.2 %.

If the confinement can be further improved, the magnetic field can be reduced. For $B_o = 6$ T and $\gamma_H = 2.5$ as shown in Fig. 6-(c), the operating point (B) can have a fusion power of ~ 3.5 GW and neutron wall loading ~ 1.8 MW/m$^2$ at $T_i(0) \sim 24.5$ keV, $n(0) \sim 2.0 \times 10^{20}$ m$^{-3}$, and $\langle\beta\rangle \sim 3.3$ %. For lower magnetic field $B_o = 5$ T and a very large confinement enhancement factor $\gamma_H = 3.5$, the operating point (A) with fusion power of ~ 3.0 GW and neutron wall loading ~ 1.5 MW/m$^2$ can exist at $T_i(0) \sim 29$ keV, $n(0) \sim 1.65 \times 10^{20}$ m$^{-3}$, and $\langle\beta\rangle \sim 4.6$ % as shown in Fig. 6-(d). In this case we notice that the density limit in the ignition regime decreases to the lower density regime due to the large confinement enhancement factor, and the density limit at the low temperature is lower than the higher magnetic field case.

**(4.3) R = 15 m reactor**

For a medium size helical reactor R = 15 m midway between the 10 m (Fig. 4-(a)) and 20 m (Fig. 6-(a)) reactors with $\bar{a} = 2$ m, $B_o = 7$ T, and $\gamma_H = 2$, the ignition regime and density limit are between these machines as shown in POPCON in Fig. 7-(a). The operating point (B) with a fusion power $P_f \sim 3.5$ GW and neutron wall loading $W_n \sim$ 2.4 MW/m$^2$ is around $T_i(0) \sim 22$ keV, $n(0) \sim 2.5 \times 10^{20}$ m$^{-3}$, and $\langle\beta\rangle \sim 2.8$ %. If the alpha particle confinement is further improved, for example up to $\eta_\alpha = 0.8$, the ignition regime expands and the operating point (A) can have a fusion power ~ 3.0 GW and neutron wall loading ~ 1.98 MW/m$^2$ at $T_i(0) \sim 21.6$ keV, $n(0) \sim 2.3 \times 10^{20}$ m$^{-3}$, and $\langle\beta\rangle \sim$ 2.5 % as shown in Fig. 7-(b).

**(4.4) POPCON for GRB Scaling in a R = 10 m Reactor**

In Fig. 8, POPCON is shown for GRB scaling in a helical reactor with R = 10 m, $\bar{a}$ = 2 m, $B_o$ = 7 T, and $\gamma_H$ = 2.2. In this case, the ignition characteristics are similar to LHD scaling with $\gamma_H$ = 2 in Fig. 4-(b). Since the confinement time saturation effect does not exist, the contour lines are continuous on both sides of the density limit line.

**(4.5) Mass effect with LHD scaling**

While the tokamak scaling and GRB scaling include the mass effect, LHD scaling does not. We have checked a possible mass factor in LHD confinement scaling such as as $(A_i/2)^{0.5}$ dependence in the deuterium experiments, and $(A_i/1.5)^{0.5}$ in the hydrogen and deuterium experiments. For a D-T plasma of $A_i$ = 2.5, the mass factors are $(A_i/2)^{0.5}$ = 1.118 or $(A_i/1.5)^{0.5}$ = 1.29, respectively. With this mass effect, the enhancement factor of $\gamma_H$ = 2.25, needed in an R = 20 m, $\bar{a}$ = 2 m, $B_o$ = 7 T helical reactor, can be reduced to $\gamma_H$ = 2.25/1.118 = 2.01 or 1.74.

**(4.6) Peaked profile effect with LHD scaling in an R = 20 m Reactor**

In general, a peaked density and temperature profile is favorable for reach ignition, because the auxiliary heating power can be reduced due to the higher fusion power and lower bremsstrahlung loss for the same average density and temperature. [15] We have examined this effect in the case $\alpha_n = \alpha_T = 2$ for an R= 20 m, $\bar{a}$ = 2 m, $B_o$ = 7 T reactor. Since the density limit shifts upward as inferred from $\gamma_{pr}$ = 15/8 in Eq.(2-18), the ignition characteristics are improved. As shown in Fig.9, the operating point with $P_f$ ~ 3 GW can be obtained at $T_i(0)$ ~ 22.5 keV, higher peak density n(0) ~ $2.6\times10^{20}$ $m^{-3}$, lower average beta value $\langle\beta\rangle$ ~ 1.8 %, and a neutron wall loading of ~ 1.5 MW/$m^2$ for the lower confinement factor $\gamma_H$ = 1.7 compared to $\gamma_H$ = 2.25 with a parabolic profile.

**(4.7) Improved density limit with LHD scaling in an R = 20 m Reactor**

We have used the confinement and density limit scaling, and assumed that

only the confinement time is improved while the density limit does not change. If the density limit can be further increased with the confinement improvement, for example, by a factor $\gamma_n = 1.5$ in Eq. (2-4), it can be taken into account replacing $\gamma_{pr}$ in Eqs. (2-18) and (2-20) with $\gamma_{pr}\gamma_n$. If the density limit increases, the Cordey pass exists below the density limit line and the auxiliary heating power can be reduced to about 30 MW as shown in Fig. 10 with R = 20 m, $\bar{a} = 2$ m, $B_o = 7$ T, $\gamma_H = 2$ and $P_{ex} = 100$ MW. The ignition regime becomes wider and the fusion power can be reduced compared to the case with the confinement enhancement factor $\gamma_H = 2$ and $\gamma_n = 1$. As shown in Fig. 10, the operating point (E) can have a fusion power $P_f \sim 2.5$ GW at $T_i(0) \sim 19.5$ keV, $n(0) \sim 2.0 \times 10^{20}$ $m^{-3}$, and $\langle\beta\rangle \sim 1.9$ %, and the operating point (A) has $P_f \sim 3.0$ GW at $T_i(0) \sim 21.0$ keV, $n(0) \sim 2.05 \times 10^{20}$ $m^{-3}$, and $\langle\beta\rangle \sim 2.1$ %. It is thus found that the density limit is an important factor to achieve ignited operation in a helical reactor. This possibility has to be examined in the coming LHD experiments.

## 5. Discussion.

We have found in this study that the confinement has to be improved more than a factor of 1.5 to reach ignition, while an enhancement factor of 2 is needed to have an optimum fusion power output ~ 3 to 4 GW for $B_o = 7$ T. Recent experiments on W-7AS has provided encouraging results with the confinement enhancement factor of 1.3.[22] To improve the confinement further by a factor of 2 to 3, high temperature divertor operation[23][24] has been proposed to raise the edge plasma temperature similar to the H-mode phenomena observed in tokamaks;[25] this will be examined in the LHD device. The limiter bias experiment has been tried to improve the confinement, but it is still at the initial stage.[26] A small Ohmic heating current has been demonstrated to improve the confinement slightly by controlling the rotational transform profile in the CHS Heliotron/Torsatron.[27] A magnetic axis shift may also improve the confinement.[28] As these techniques have not yet been successful to improve the confinement up to a factor of 2, further experimental efforts is needed for

developing a helical reactor.

We have also seen that the volume averaged beta value with respect to the magnetic field $B_0$ ranges from 3 to 5 % in the ignition regime, depending on the magnetic field strength. As the highest <β> value so far obtained is 2.0 % in the Heliotron-E device,[29] additional experimental effort is needed for the further increase in the beta value by a factor two.

We have only used the empirical scaling and the global power balance equation with equal electron and ion confinement times. Therefore, the global power balance analyses are only applicable when the confinement is improved for both species equally. (If these two confinement times are different and either confinement is improved, the power balance equations for ions and electrons have to be solved simultaneously.) In this study, the confinement time has been arbitrarily assumed larger by an enhancement factor with respect to the empirical scaling, and no account has been taken of a particular helical configuration. The neoclassical ion confinement time $\tau_{E,NEO}$ due to ripple trapped particles with a negative electric field is of primary concern in a helical system and is given by[11]

$$\tau_E[s] = 0.11\ \bar{n}[\times 10^{20}\ m^{-3}]\ B_o^{4/9}[T]\ \bar{a}^2[m]\ R^{11/9}[m]\ \varepsilon_h^{-1/3}/P_H^{7/9}[MW]\ . \qquad (5\text{-}1)$$

It provides 3.57 sec for a helical ripple $\varepsilon_h = 0.02$, and 2.1 sec for $\varepsilon_h = 0.1$ in the case of R = 20 m, $\bar{a}$ = 2 m, $B_0$ = 7 T, $\bar{n} = 2\times10^{20}\ m^{-3}$, and $P_H$ = 300 MW. These values are, respectively, comparable to and a half of the LHD confinement time $\tau_{E,LHD}$ = 3.89 sec with an enhancement factor of 2. Since the neoclassical loss may limit the confinement enhancement factor to a lower value as estimated here, further optimization of a helical reactor is needed to have a large neoclassical confinement time with a small helical ripple[30], and experiments to improve the confinement should be continued actively.

## 6. Summary

We have surveyed various sizes of D-T helical reactors reaching ignition and operating in the ignition regime with LHD and GRB scalings using the operation path method and "POPCON". In the case of fixed parameters such as $\alpha_T = \alpha_n = 1$, $Z_{eff} = 1.5$, $f_\alpha = 0.05$, $\eta_\alpha = 0.7$, and $T_i(0)/T_e(0) = 1$, we have found the following.

A helical reactor with $R > 8$ m and $\bar{a} \sim 2$ m, a magnetic field strength $B_0 > 6$ T, and a confinement enhancement factor > 1.5 can reach ignition, but an optimum fusion power output (~ 3 to 3.5 GW) needs a confinement enhancement factor such as $\gamma_H > 2$. As the magnetic field strength is increased, the required confinement enhancement factor $\gamma_H$ can be reduced.

The density limit scaling and confinement time saturation effect with respect to the density have been demonstrated to be the important limiting factors for ignition in a helical reactor. The improvement of the density limit is very helpful as is the confinement improvement.

For GRB scaling, an confinement enhancement factor $\gamma_H = 2.2$ is needed to have the same ignition capability as LHD scaling with $\gamma_H = 2$ for an $R = 10$ m, $\bar{a} = 2$ m and $B_0 = 7$ T reactor. The confinement time saturation effect with respect to the density does not exist for GRB scaling, and confinement is not improved with an increase in the major radius.

Ignition plasma parameters at the operating point for R=10 m, 15 m, and 20 m helical reactors with LHD scaling are summarized in Table 2. With the increase in major radius of a reactor, the ignition regime becomes wider due to the better confinement, and the plasma density and operating beta value can be reduced for the same confinement enhancement factor. While the total fusion power increases due to the larger plasma volume for the same plasma parameters, the neutron wall loading is reduced due to the larger surface area of the vacuum chamber. Thus, in a larger reactor, the beta value, operating density and neutron wall loading can be reduced even for the larger fusion power as long as the same value of the confinement enhancement factor

can be obtained.

## Appendix

Notations $A_L$, $A_\alpha$, and $A_b$ in Eqs. (2-8) and (2-9) are given as follows: The coefficient for the plasma conduction loss is $A_L = 1.5\,(f_D + f_T + 1/\gamma_i)\,T_i(0)\,1.6\times10^{-19}/(1+\alpha_n+\alpha_T)$ with $\gamma_i = T_i(0)/T_e(0)$, $f_D = n_D(0)/n(0)$, $f_T = n_T(0)/n(0)$, $f_D = f_T = 0.5 - \{(Z-2)/(Z-1)\}f_\alpha - \{(Z_{eff}-1)/(Z-1)\}0.5$, $Z_{eff} = 1 + 2f_\alpha + Z(Z-1)f_z$, $f_z = n_z(0)/n(0)$ is the impurity fraction and Z = 7. The coefficient for the alpha particle heating is $A_\alpha = f_D f_T (3.52\eta_\alpha)\overline{<\sigma v>}_{DT}1.6\times10^{-13}$ where $\eta_\alpha$ is the alpha particle fraction, and the coefficient for the bremsstrahlung loss is $A_b = 1.5\times10^{-38}Z_{eff}\{T_i(0)/\gamma_i\}^{0.5}/(1 + 2\alpha_n + 0.5\alpha_T)$. The electron density and temperature profiles are assumed to be $n(x) = n(0)\,(1-x^2)^{\alpha_n}$ and $T_i(x)/T_i(0) = T_e(x)/T_e(0) = (1-x^2)^{\alpha_T}$.


## Acknowledgements

One of authors (O.M.) gratefully acknowledges Prof. H.M.Skarsgard, Canada, for reading this paper, and all the Faculty members in the Department of Electrical Engineering, Kumamoto Institute of Technology, for encouragement. One of authors (O.M.) also thanks Prof. M.Fujiwara for critical comments, and Dr. A.Sagara, Prof. O.Motojima and Prof. A.Iiyoshi for continuous interest in this work.

## References


1. D.A.EHST, K.EVANS, Jr., and M.KLASKY, "rf Generation of Stable High Bootstrap Current Equilibria," *Phys. Rev. Lett.*, **64**, 1891 (1990).
2. O.MITARAI, S.W.WOLFE, A.HIROSE, and H.M.SKARSGARD, "Stable AC Tokamak Discharge in the STOR-1M Device," Bull. Am. Phys. Society, **6V3**, (Oct. 1984, Boston) 1337, and *Nucl. Fusion*, **27**, 604 (1987), O.MITARAI, S.W.WOLFE, A.HIROSE, and H.M.SKARSGARD, "Alternating Current Tokamak Reactor With Long Pulses," *Fusion Technology*, **15**, 204 (1989), O.MITARAI, A.HIROSE, and H.M.SKARSGARD, "Alternating Current Tokamak Reactor With Ohmic Ignition and Bootstrap Current," *Fusion Technology*, **20**, 285 (1991), and O.MITARAI, A.HIROSE, and H.M.SKARSGARD, "Plasma Density at the Current Reversal in the STOR-1M Tokamak with AC Operations," *Nucl. Fusion*, **32**,1801 (1992).
3. S.C.JARDIN, "Physics Overview of CIT," in *13th Symposium on Fusion Engineering*, (Oct. 1989, Knoxville, USA), Vol.2, 1265.
4. R.TOSCHI, M.CHAZALON, F.ENGELMANN, J.NIHOUL, J.RAEDER, and E.SALPIETRO, "Next European Torus Objective, General Requirements, and Parameter Choices," *Fusion Technology*, **14**, 19 (1988).
5. M.SUGIHARA, N.FUJISAWA, H.IIDA, S.NISHIO, Y.SEKI, et al., "Design Study of Fusion Experimental Reactor," in *12th Int. Conf. on Plasma Physics and Controlled Nucl. Fusion Research*, IAEA-CN-50/G-1-2, Nice, France, Oct. 1988.
6. J.R.GILLELAND, Yu.A.SOKOLOV, K.TOMABECHI, and R.TOSCHI, "ITER; Concept Definition," *Nucl. Fusion*, **29**, 1191 (1989).
7. I.YANAGISAWA, N.UEDA, M.YAMADA, R.SAITO, T.YAMADA, M.TOMITA, H.NAKASHIMA, O.MOTOJIMA, M.NAKASUGA, A.IIYOSHI, K.UO, "A Design Study of a Heliotron Power Reactor," *Nuclear Technology/ Fusion*, **4**, 1302 (1983).
8. W.A.HOULBERG, J.T.LACATSKI, N.A.UCKAN, "Assessment of A Compact

Torsatron Reactor, ATFSR," *Fusion Technology*, **10**, 227 (1986).

9. J.F.LYON, B.A.CARRERAS, V.E.LYNCH, J.S.TOLLIVER, and I.N.SVIATOSLAVSKY, "Compact Torsatron Reactors," *Fusion Technology*, **15**, 227 (1989).

10. S.L.PAINTER, and J.F. LYON, "Transport Analysis of Stellarator Reactors," *Nucl. Fusion*, **31**, 2271 (1991).

11. S.SUDO, Y.TAKEIRI, H.ZUSHI, F.SANO, K.ITOH, K.KONDO, and A.IIYOSHI, "Scalings of Energy Confinement and Density Limit in Stellarator/Heliotron Devices," *Nucl.Fusion*, **30**, 11 (1990).

12. M.MURAKAMI, S.C.ACETO, et al., "Recent results from the ATF torsatron," *Phys. Fluids* B **3** (8), 2261 (1991).

13. H.RENNER, U.GASPARINO, et al., "Confinement Properties of the 'Advanced Stellarator' Wenderstein W 7AS," in *13th Int. Conf. on Plasma Physics and Controlled Nucl. Fusion Research*, IAEA-CN-53/C-1-2, Washington, DC, USA, Oct. 1990.

14. O.MITARAI, A.HIROSE, and H.M.SKARSGARD, "Generalized Ignition Contour Map and Scaling Law Requirement For Reaching Ignition in a Tokamak Fusion Reactor," *Nucl. Fusion*, **28**, 2141 (1988).

15. O.MITARAI, A.HIROSE, and H.M.SKARSGARD, "Generalized Saddle Point Condition for Ignition in a Tokamak Reactor with Temperature and Density Profiles," *Fusion Technology*, **16**, 197 (1989).

16. O.MITARAI, A.HIROSE, and H.M.SKARSGARD, "Ignition Access Condition Based on the Generalized Saddle Point in a Magnetic Fusion Reactor," *Fusion Technology*, **20**, 208 (1991).

17. O.MITARAI, A.HIROSE, and H.M.SKARSGARD, "Operation Path Method for Ignition Criterion in a D-T Tokamak Reactor," *Fusion Technology*, **22**, 227 (1992).

18. W.A.HOULBERG, S.E.ATTENBERGER, and L.M.HIVELY, "Contour Analysis

of Fusion Reactor Plasma Performance," *Nucl. Fusion*, **22**, 935 (1982), and N.A.UCKAN, and J.SHEFFIELD, "A Simple Procedure For Establishing Ignition Conditions in Tokamaks," in Tokamak Start-up Problems and Scenarios Related to the Transient Phases of a Thermonuclear Fusion Reactor, (Ed.by H.KNOEPFEL, Plenum Press, New York, 1986) 45.

19. S.L.PAINTER, and J.F. LYON, "Alpha-Particle Losses in Compact Torsatron Reactors,"*Fusion Technology*, **16**, 157 (1989).

20. S.SUDO, H.ZUSHI, F.SANO, K.KONDO, T.MIZUUCHI,S.BESSHOU, T.BABA, M.WAKATANI, T.OBIKI, and H-E Group, "Density Profile Effects on Transport and MHD Stability of Heliotron E NBI Plasmas," Bulletin of the Physical Society of Japan, 28p-Z-3, p184 (Keio University, May, 1992).

21. N.A.UCKAN and ITER Physics Group, "ITER Physics Design Guidelines," ITER-TN-PH-8-6 (1988), and N.A.UCKAN, J.S.TOLLIVER, W.A.HOULBERG, and S.E.ATTENBERGER, "Influence of fast Alpha Diffusion and Thermal Alpha Buildup on Tokamak Reactor Performance," *Fusion Technology*, **13**, 411 (1988).

22. V.ERCKMANN, F.WAGNER, J.BALDZUHN, R.BRAKET, R.BURHENN, et al., "H Mode of the W 7-AS Stellarator," *Phys. Rev. Lett.*, **70**, 2086 (1993).

23. N.OHYABU, "High Temperature Divertor Plasma Operation," Kakuyuugo-Kenkyu, The Japan Society of Plasma Science and Nuclear Fusion Research, **66**, 525 (1991).

24. N.OHYABU, K.YAMAZAKI, I.KATANUMA, H.JI, T.WATANABE, et al., "Design Study of LHD Helical Divertor and High Temperature Divertor Plasma Operation," in 14*th Int. Conf. on Plasma Physics and Controlled Nucl. Fusion Research*, (WÜrzburg, Germany, 1992), IAEA-CN-56/C-4-2.

25. F.WAGNER, G.BECKER, K.BEHRINGER, D.CAMPBELL, A.EBERHAGEN, et al., "Regime of Improved Confinement and High Beta in Neutral-Beam-Heated Divertor Discharges of the ASDEX Tokamak," *Phys. Rev. Lett.*, **64**, 1408

(1982).

26. R.C.ISLER, S.ACETO, L.R.BAYLOR, T.S.BIGELOW, G.L.BELL et al., "Effects of Magnetic Geometry, Fluctuations, and Electric Fields on Confinement in the Advanced Toroidal Facility," *Phys. of Fluids*, B **4** (7), 2104 (1992).

27. K.TOI, S.OKAMURA, H.IGUCHI, H.YAMADA, S.MORITA, et al., "Formation of H-mode Like Transport Barrier in the CHS Heliotron/ Torsatron," in 14*th Int. Conf. on Plasma Physics and Controlled Nucl. Fusion Research*, (Würzburg, Germany, 1992), IAEA-CN-56/H-1-3 (post-deadline paper).

28. T.OBIKI, S.SUDO, F.SANO, K.KONDO, M.NAKASUGA, et al., "Confinement Improvement in ECH and NBI Heated Heliotron E Plasmas," in 13*th Int. Conf. on Plasma Physics and Controlled Nucl. Fusion Research*, (Washington, DC, USA, 1990), IAEA-CN-53/C-1-1.

29. O.MOTOJIMA, F.SANO, M.SATO, H.KANEKO, H.ZUSHI, S.SUDO, S.BESSHOU, A.SASAKI, K.KONDO, T.MUTOH, T.MIZUUCHI, H.OKADA, M.IIMA, T.BABA, K.HANATANI, J.H.HARRIS, M.WAKATANI, T.OBIKI, A.IIYOSHI, K.UO, "Studies of Currentless, High-Beta Plasma in the Heliotron E Device," *Nucl. Fusion*, **25**, 1783 (1985).

30. G.GRIEGER, W.LOTS, P.MERKEL, J.NÜHRENBERG, J.SAPPER, E.STRUMBERGER, H.MOBIG, and the W7-X Team et al., "Physics Optimization of Stellarators," *Phys. of Fluids*, B **4** (7), 2081 (1992).

## Figure Captions

Fig.1 The confinement time saturation effect with respect to the electron density for LHD scaling and the reference reactor R = 10 m, $\bar{a}$ = 2 m, $B_0$ = 7 T, $\gamma_H$ = 2, and T(0) = 10 keV. The plasma parameters $\eta_\alpha$ = 0.7, $\alpha_n = \alpha_T$ = 1, $T_i(0)/T_e(0)$ = 1, $Z_{eff}$ = 1.5, $f_\alpha$ = 0.05, Z = 7 and $f_D = f_T$ = 0.415 are used throughout the paper unless otherwise noted. The density limit can be determined by the intersection point given by Eq.(2-18) and then $n_{SH}(0)$ is determined. The solid line is for $\gamma_S$ = 0.6 and the dashed line for $\gamma_S$ = 1, where the calculation was performed from the larger $n_{lim}(0)$ value to smaller one.

Fig.2 Ignition boundary $[\bar{P}_{ht}\tau_E^2]_{ig}$ and operation paths $[\bar{P}_{ht}\tau_E^2]_{op}$ for LHD and GRB scalings with R = 10 m, $\bar{a}$ = 2 m, and $B_0$ = 7 T. The confinement enhancement factors $\gamma_H$ = 1.5 and 2 and the alpha particle confinement fractions $\eta_\alpha$ = 0.7 to 1.0 are specified. Other plasma parameters are the same as in Fig.1.

Fig.3 Ignition boundaries for $\alpha_n$ = 1 and 0.5 and operation paths for the various sizes of helical reactor with $\bar{a}$ = 2 m and $\bar{n} = 2\times10^{20}$ $m^{-3}$ in the case of (a) $B_0$ = 7 T and $\gamma_H$ = 2, (b) $B_0$ = 6 T and $\gamma_H$ = 2, and (c) $B_0$ = 8 T and $\gamma_H$ = 1.5. Other plasma parameters are the same as in Fig.1.

Fig.4 "POPCON" analyses for the helical reactor R = 10 m, $\bar{a}$ = 2 m, $B_0$ = 7 T, $\gamma_H$ = 2 and LHD scaling (a) with and (b) without the confinement time saturation effect with respect to the density. The operating points (A), (B), and (C) correspond to the fusion power $P_f$ = 3.0, 3.5 and 4.0 GW, respectively. $P_{ex}$ = 100 MW and other plasma parameters are the same as in Fig.1.

Fig.5 "POPCON" analyses for the helical reactor R = 10 m, $\bar{a}$ = 2 m and LHD scaling in the case of (a) $B_0$ = 6 T and $\gamma_H$ = 2, and (b) $B_0$ = 8 T and $\gamma_H$ = 1.5. $P_{ex}$ = 100 MW and other plasma parameters are the same as in Fig.1.

Fig.6 "POPCON" analyses for the helical reactor R = 20 m, $\bar{a}$ = 2 m and LHD scaling in the case of (a) $B_0$ = 7 T and $\gamma_H$ = 2, (b) $B_0$ = 7 T and $\gamma_H$ = 2.25, (c) $B_0$ = 6 T and $\gamma_H$ = 2.5, and (d) $B_0$ = 5 T and $\gamma_H$ = 3.5. The operating points (A), (B), and (C)

correspond to the fusion power $P_f$ = 3.0, 3.5 and 4.0 GW, respectively. $P_{ex}$ = 100 MW and other plasma parameters are the same as in Fig.1.

Fig.7 "POPCON" analyses for the helical reactor R = 15 m, $\bar{a}$ = 2 m and LHD scaling in the case of (a) $B_0$ = 7 T and $\gamma_H$ = 2, and (b) the improved alpha particle confinement for the same parameters as in (a) except for $\eta_\alpha$ = 0.8. The operating points (A), (B), and (C) correspond to the fusion power $P_f$ = 3.0, 3.5 and 4.0 GW, respectively. $P_{ex}$ = 100 MW and other plasma parameters are the same as in Fig. 1.

Fig.8 "POPCON" analysis with GRB scaling for the helical reactor R = 10 m, $\bar{a}$ = 2 m, $B_0$ = 7 T, and $\gamma_H$ = 2.2. The operating points (A), (B), and (C) correspond to the fusion power $P_f$ = 3.0, 3.5 and 4.0 GW, respectively. $P_{ex}$ =100 MW and other plasma parameters are the same as in Fig.1.

Fig.9 "POPCON" analysis with peaked density and temperature profile ($\alpha_n = \alpha_T = 2$) for a reactor of R = 20 m, $\bar{a}$ = 2 m, $B_0$ = 7 T, and LHD scaling. The confinement enhancement factor can be reduced to $\gamma_H$ = 1.7, compared to 2.25 for the parabolic profile, to have a fusion power of $P_f$ = 3 GW. The operating points (A), (B) and (C) correspond to the fusion power $P_f$ = 3.0, 3.5, and 4.0, respectively. $P_{ex}$ = 100 MW and other plasma parameters are the same as in Fig.1.

Fig.10 "POPCON" analysis for the same parameters in Fig. 6-(a) (with R = 20 m, $\bar{a}$ = 2 m, $B_0$ = 7 T, $\gamma_H$ = 2, and LHD scaling) except for the improved density limit scaling with $\gamma_n$ = 1.5. The operating points (E), (A), and (B) correspond to the fusion power $P_f$ = 2.5, 3.0, and 3.5, respectively. $P_{ex}$ = 100 MW and other plasma parameters are the same as in Fig.1.

| | R (m) | $\bar{a}$ (m) | A | $B_o$ (T) | $V_o$ ($m^3$) | $C_{op}^2$(LHD) $(MW/m^3s^2)^{1.16}$ | $C_{op}^2$(GRB) $(MW/m^3s^2)^{1.2}$ |
|---|---|---|---|---|---|---|---|
| [Low aspect ratio] A ≤ 5 | | | | | | | |
| HELICAR-LA1 | 10 | 2 | 5 | 6.0 | 790 | 0.129 | 0.113 |
| | | | | 7.0 | | 0.167 | 0.145 |
| | | | | 8.0 | | 0.209 | 0.179 |
| HELICAR-LA2 | 8 | 2 | 4 | 6.0 | 632 | 0.120 | 0.113 |
| | | | | 7.0 | | 0.155 | 0.145 |
| | | | | 8.0 | | 0.194 | 0.179 |
| [High aspect ratio] A > 7 | | | | | | | |
| HELICAR-HA1 | 20 | 2 | 10 | 6.0 | 1579 | 0.164 | 0.113 |
| | | | | 7.0 | | 0.212 | 0.145 |
| | | | | 8.0 | | 0.265 | 0.179 |
| HELICAR-HA2 | 15 | 2 | 7.5 | 6.0 | 1184 | 0.148 | 0.113 |
| | | | | 7.0 | | 0.192 | 0.145 |
| | | | | 8.0 | | 0. 240 | 0.179 |
| Heliotron[5] | 21.0 | 1.8 | 11.7 | 4.0 | 1343 | 0.070 | 0.046 |
| | | | | 6.0 | | 0.139 | 0.088 |
| | | | | 8.0 | | 0.226 | 0.139 |

Table 1. Machine parameters and the operation path parameters in proposed helical reactors. A line-averaged density $\bar{n} = 1 \times 10^{20}\ m^{-3}$ is taken for calculating $C_{op}^2$ with $\gamma_H = 1$. For calculation of $C_{op}^2$(GRB), $\kappa = 1$ and $a = \bar{a}$ are assumed.

| | R (m) | $\bar{a}$ (m) | $\gamma_H$ | $P_f$ (GW) | $W_n$ ($MW/m^2$) | n(0) ($x10^{20}m^{-3}$) | $T_i(0)$ (keV) | $<\beta>$ (%) | $\alpha_n=\alpha_T$ | $\gamma_n$ |
|---|---|---|---|---|---|---|---|---|---|---|
| HELICAR-LA1 | 10 | 2 | 2 | 3.4 | 3.5 | 2.9 | 23.0 | 3.3 | 1 | 1 |
| HELICAR-HA2 | 15 | 2 | 2 | 3.5 | 2.4 | 2.5 | 22.0 | 2.8 | 1 | 1 |
| HELICAR-HA1 | 20 | 2 | 2 | 4.0 | 2.0 | 2.3 | 22.0 | 2.5 | 1 | 1 |
| | | | 2.25 | 3.0 | 1.5 | 1.9 | 23.5 | 2.2 | 1 | 1 |
| | | | 1.7 | 3.0 | 1.5 | 2.6 | 22.5 | 1.8 | 2 | 1 |
| | | | 2 | 2.5 | 1.25 | 2.0 | 19.5 | 1.9 | 1 | 1.5 |

Table 2. Machine size and plasma parameters at the operating point with LHD scaling in three helical reactors with $B_o$= 7 T. $P_f$: the fusion power, $W_n$: the neutron wall loading, and $\gamma_n$: density limit improvement factor.

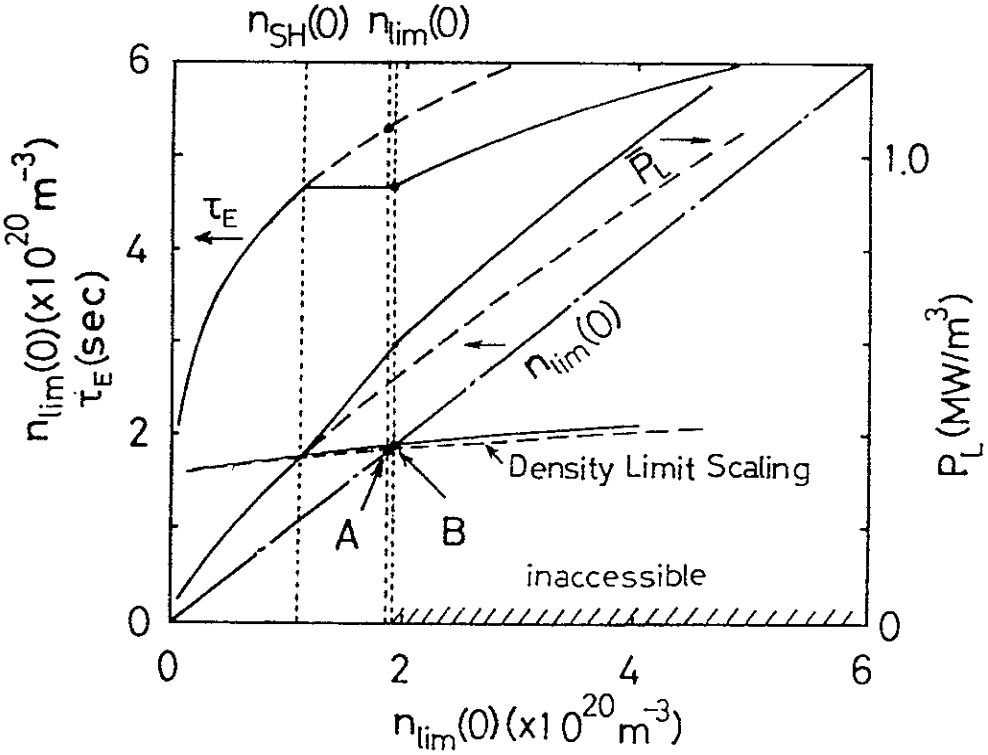
$n_{SH}(0)$ $n_{lim}(0)$
$n_{lim}(0)(x10^{20}m^{-3})$
$\tau_E(sec)$
$\tau_E$
$\bar{P}_L$
$n_{lim}(0)$
Density Limit Scaling
A
B
inaccessible
$P_L(MW/m^3)$
$n_{lim}(0)(x10^{20}m^{-3})$

Fig. 1

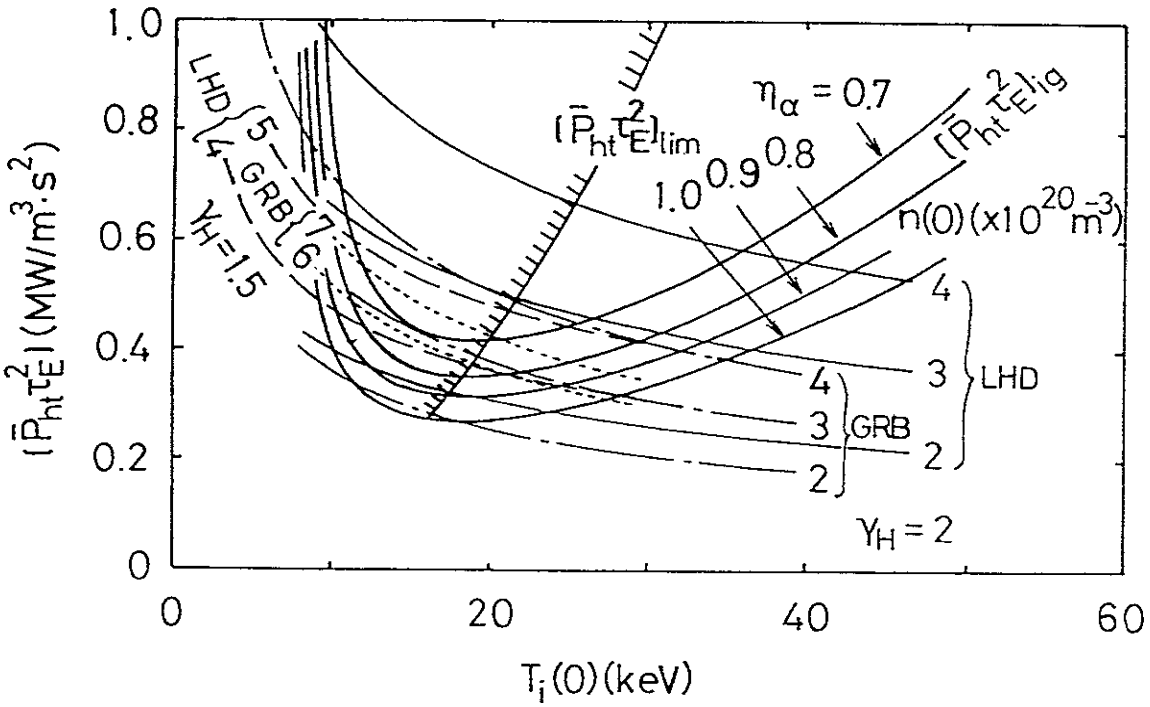
$(\bar{P}_{ht}\tau_E^2)(MW/m^3\cdot s^2)$
LHD
GRB
$\gamma_H$=1.5
$(\bar{P}_{ht}\tau_E^2)_{lim}$
$\eta_\alpha$ = 0.7
1.0 0.9 0.8
$(\bar{P}_{ht}\tau_E^2)_{ig}$
$n(0)(x10^{20}m^{-3})$
LHD
GRB
$\gamma_H$ = 2
$T_i(0)(keV)$

Fig. 2

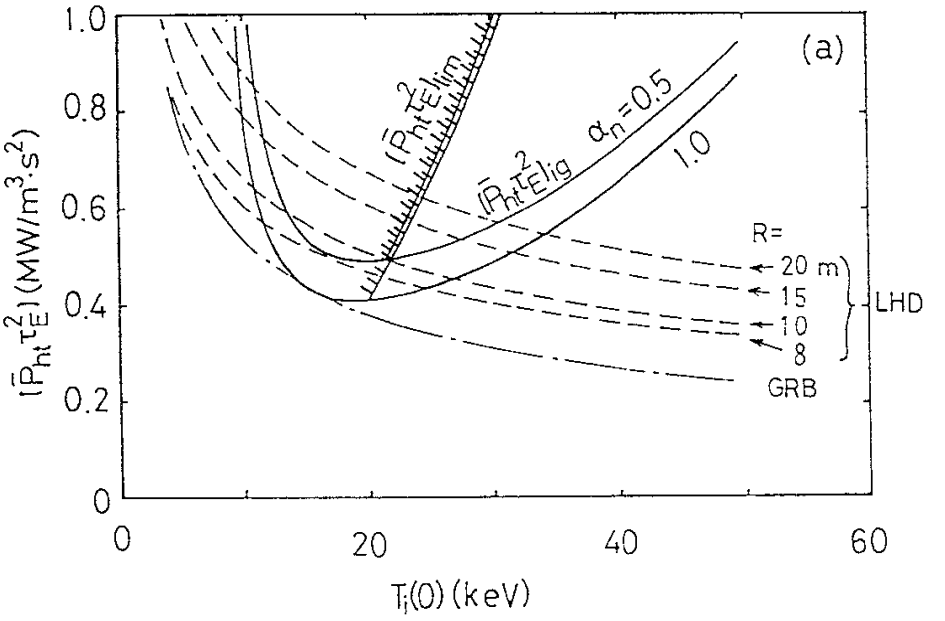
(a)
$(\bar{P}_{ht}\tau_E^2)_{lim}$
$(\bar{P}_{ht}\tau_E^2)_{lig}$
$\alpha_n$=0.5
1.0
R=
20 m
15
10
8
GRB
LHD
$(\bar{P}_{ht}\tau_E^2)$ (MW/m$^3$·s$^2$)
$T_i(0)$ (keV)

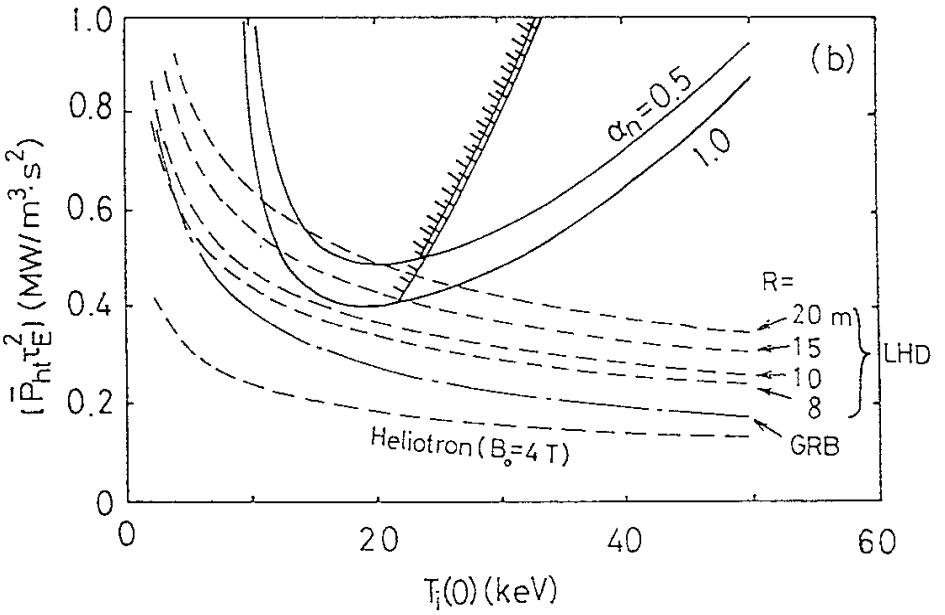
(b)
$\alpha_n$=0.5
1.0
R=
20 m
15
10
8
GRB
LHD
Heliotron ($B_o$=4 T)
$(\bar{P}_{ht}\tau_E^2)$ (MW/m$^3$·s$^2$)
$T_i(0)$ (keV)

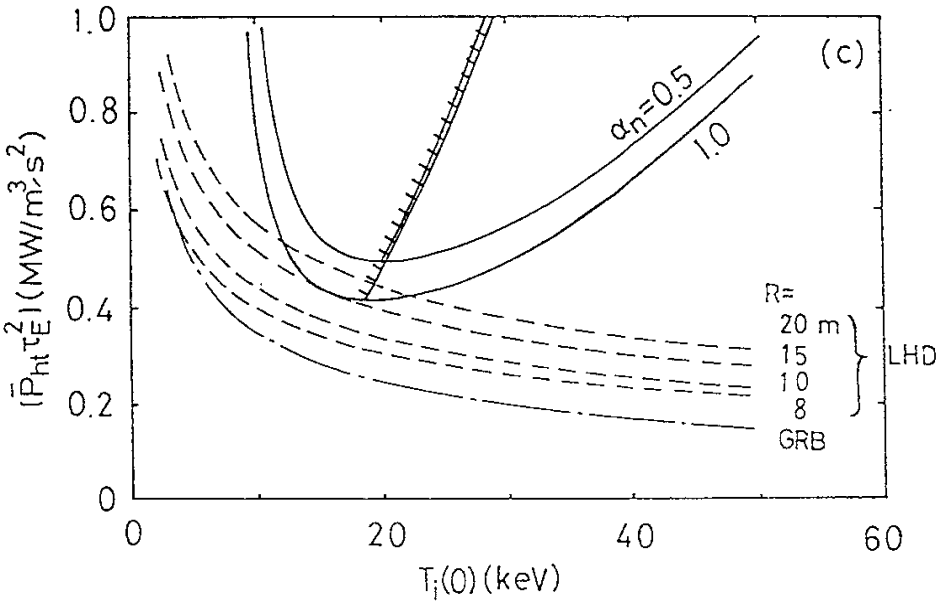
(c)
$\alpha_n$=0.5
1.0
R=
20 m
15
10
8
GRB
LHD
$(\bar{P}_{ht}\tau_E^2)$ (MW/m$^3$·s$^2$)
$T_i(0)$ (keV)

Fig. 3-(a),(b),(c)

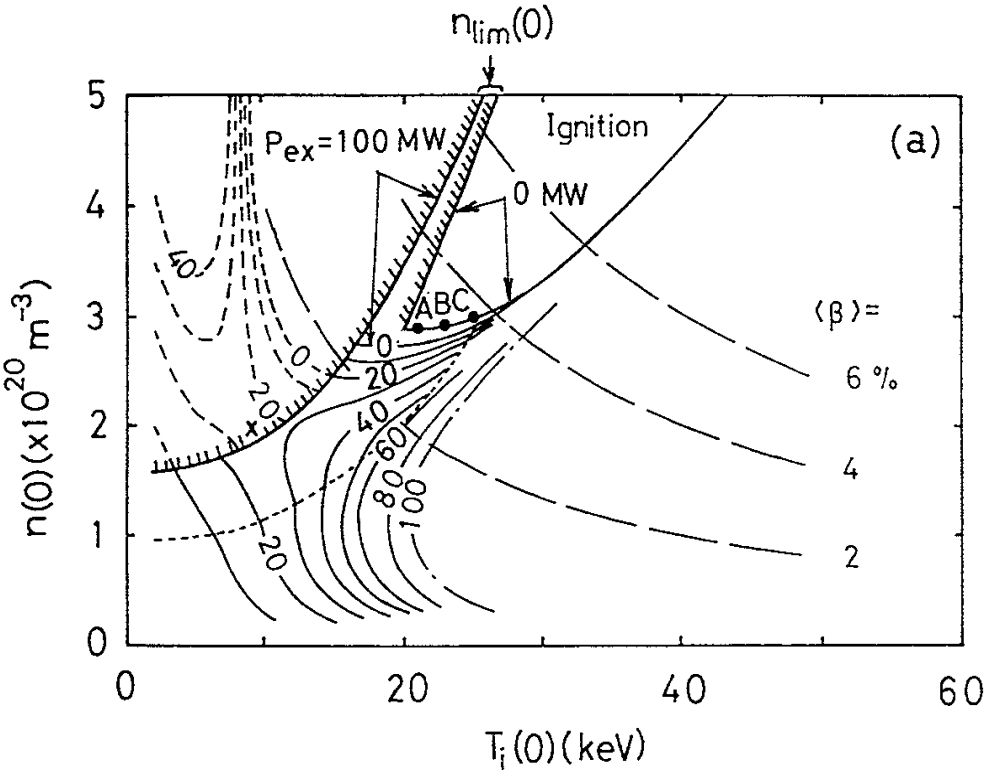
$n_{lim}(0)$
Ignition
(a)
$P_{ex}$=100 MW
0 MW
ABC
⟨β⟩=
6 %
4
2
50
0
20
40
60
80
100
$n(0)(x10^{20}\,m^{-3})$
$T_i(0)$(keV)

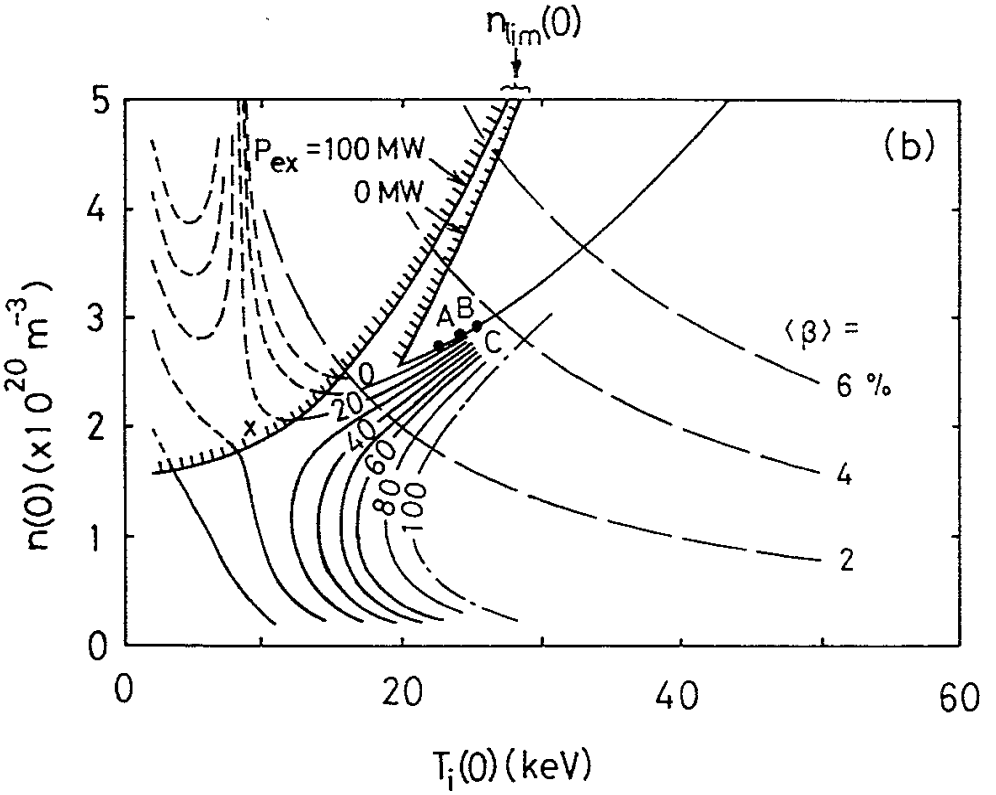
$n_{lim}(0)$
(b)
$P_{ex}$ =100 MW
0 MW
AB
C
⟨β⟩ =
6 %
4
2
0
20
40
60
80
100
$n(0)(x10^{20}\,m^{-3})$
$T_i(0)$(keV)

Fig. 4-(a),(b)

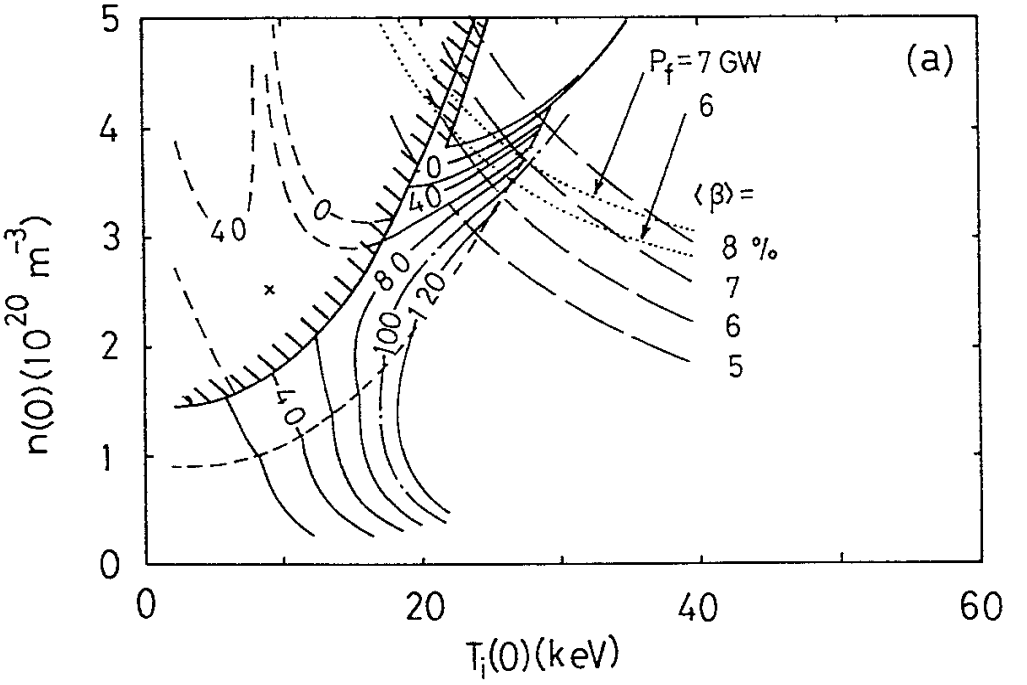
(a)
$P_f$ = 7 GW
6
⟨β⟩ =
8 %
7
6
5
0
40
80
120
100
n(0)($10^{20}$ $m^{-3}$)
$T_i$(0)(keV)

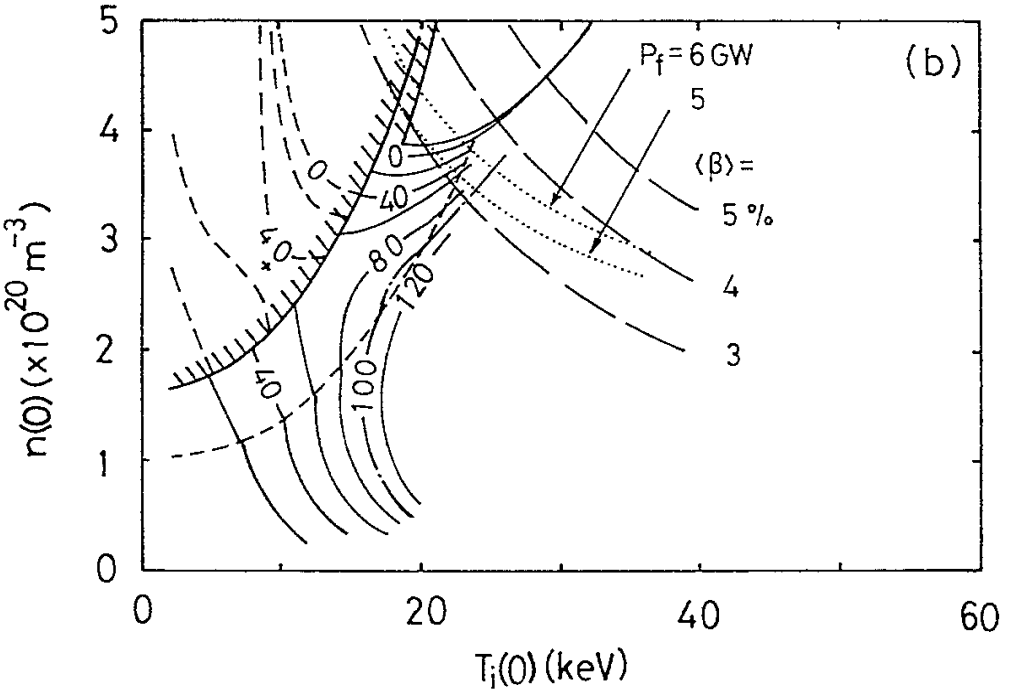
(b)
$P_f$ = 6 GW
5
⟨β⟩ =
5 %
4
3
0
40
80
120
100
n(0)(x$10^{20}$ $m^{-3}$)
$T_i$(0) (keV)

Fig. 5-(a),(b)

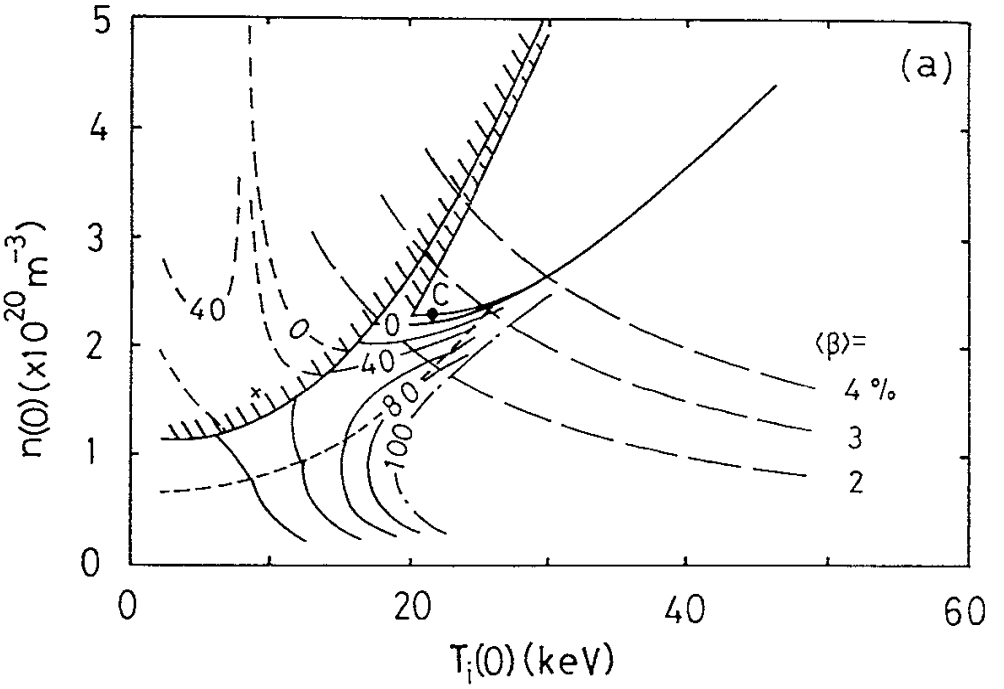
(a)
n(0)(x10^20 m^-3)
T_i(0)(keV)
C
40
0
0
40
80
100
⟨β⟩=
4 %
3
2

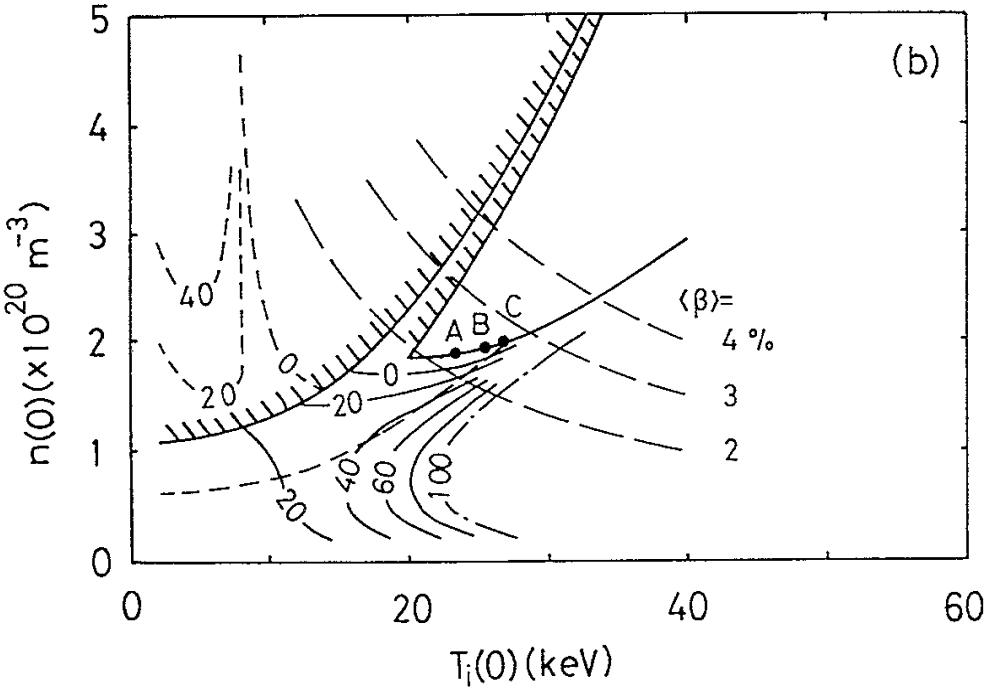
(b)
n(0)(x10^20 m^-3)
T_i(0)(keV)
A
B
C
40
20
0
0
20
20
40
60
100
⟨β⟩=
4 %
3
2

Fig. 6-(a),(b)

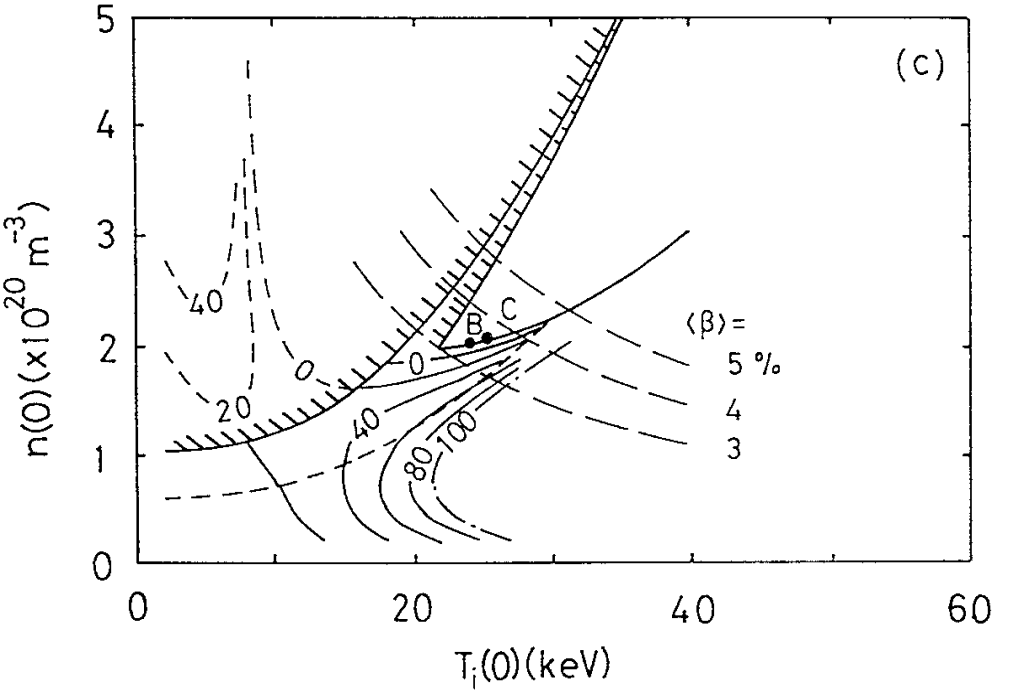
(c)
n(0)(x10^20 m^-3)
T_i(0)(keV)
⟨β⟩=
5 %
4
3
B
C
40
20
0
0
40
80
100

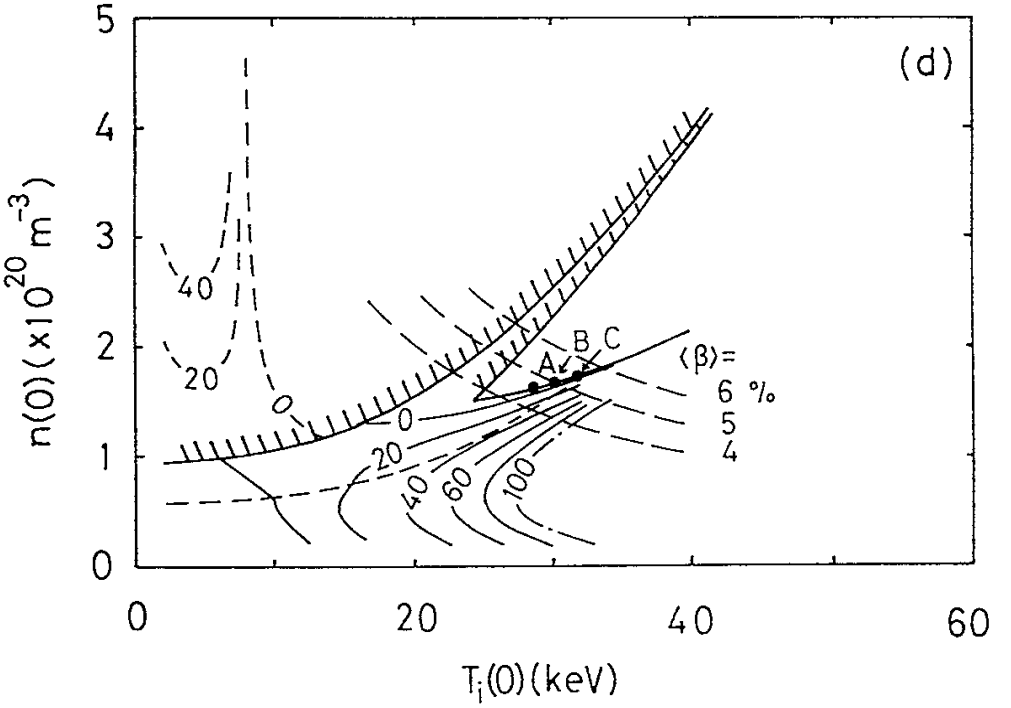
(d)
n(0)(x10^20 m^-3)
T_i(0)(keV)
⟨β⟩=
6 %
5
4
A
B
C
40
20
0
0
20
40
60
100

Fig. 6-(c),(d)

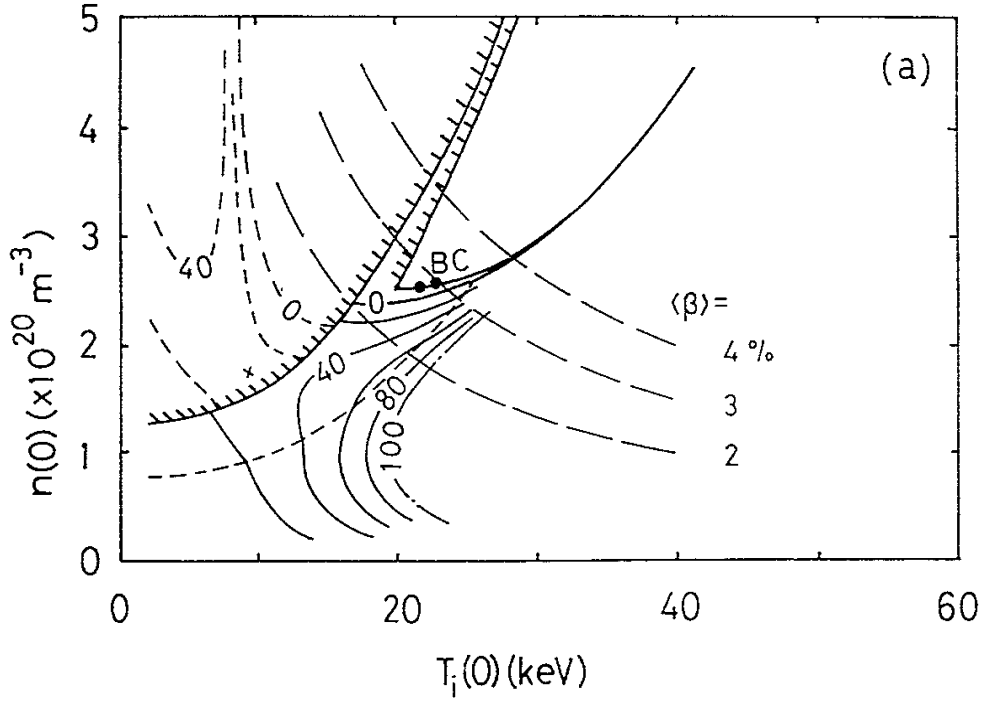
(a)
n(0) (x10^20 m^-3)
T_i(0) (keV)
BC
40
0
0
40
80
100
x
⟨β⟩=
4 %
3
2
0
1
2
3
4
5
0
20
40
60

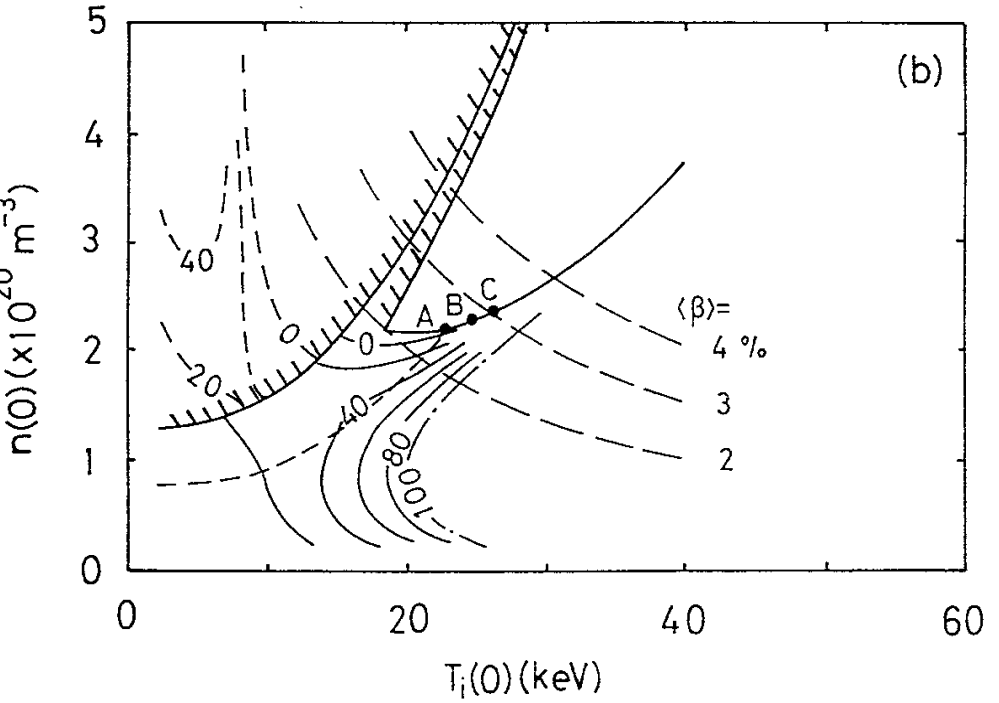
(b)
n(0) (x10^20 m^-3)
T_i(0) (keV)
A
B
C
40
0
0
20
40
80
100
⟨β⟩=
4 %
3
2
0
1
2
3
4
5
0
20
40
60

Fig. 7-(a),(b)

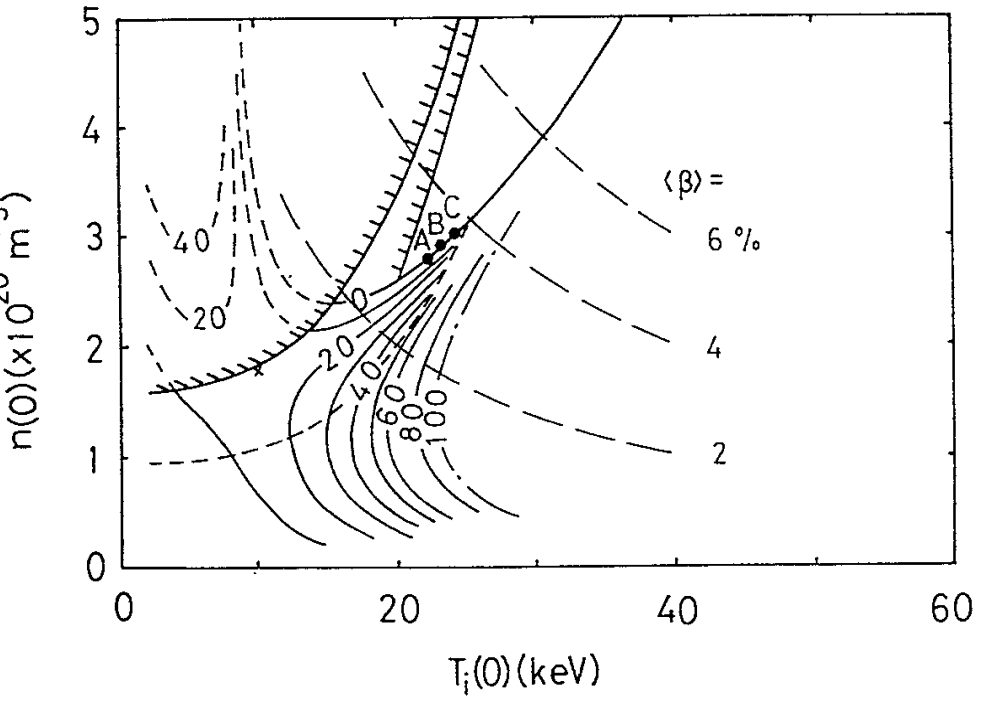
n(0)(x10^20 m^-3)
T_i(0)(keV)
⟨β⟩ =
6 %
4
2
A
B
C
0
20
40
60
80
100

Fig. 8

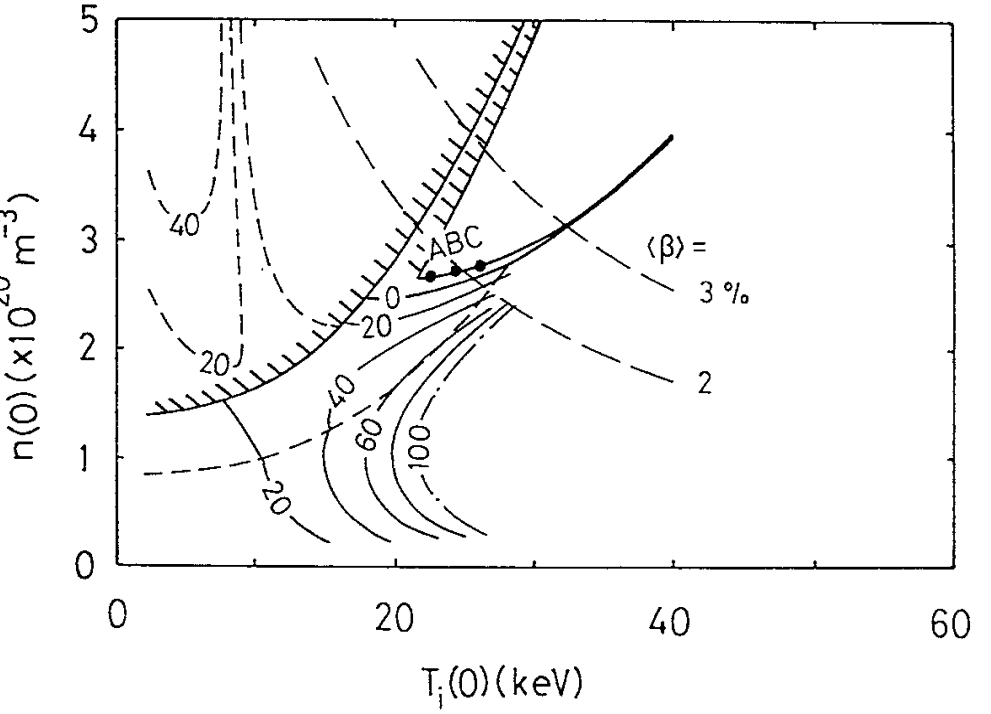
n(0)(x10^20 m^-3)
T_i(0)(keV)
⟨β⟩ =
3 %
2
A
B
C
0
20
40
60
100

Fig. 9

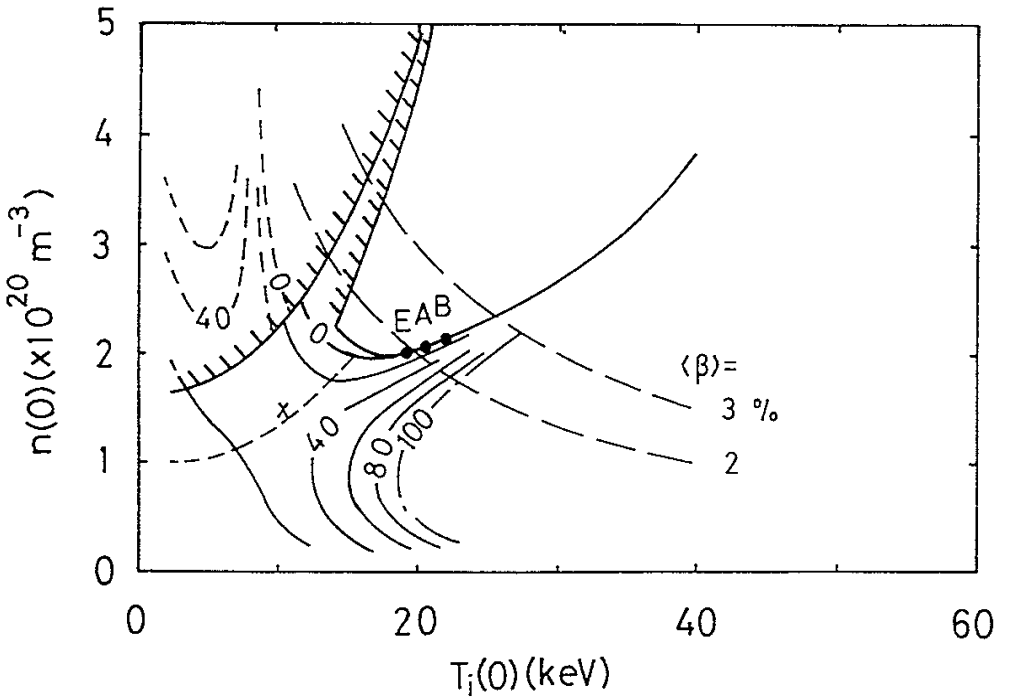


Fig. 10

## Recent Issues of NIFS Series

NIFS-238 K. Watanabe, T. Sato and Y. Nakayama, *Q-profile Flattening due to Nonlinear Development of Resistive Kink Mode and Ensuing Fast Crash in Sawtooth Oscillations;* July 1993

NIFS-239 N. Ohyabu, T. Watanabe, Hantao Ji, H. Akao, T. Ono, T. Kawamura, K. Yamazaki, K. Akaishi, N. Inoue, A. Komori, Y. Kubota, N. Noda, A. Sagara, H. Suzuki, O. Motojima, M. Fujiwara, A. Iiyoshi, *LHD Helical Divertor;* July 1993

NIFS-240 Y. Miura, F. Okano, N. Suzuki, M. Mori, K. Hoshino, H. Maeda, T. Takizuka, JFT-2M Group, K. Itoh and S.-I. Itoh, *Ion Heat Pulse after Sawtooth Crash in the JFT-2M Tokamak;* Aug. 1993

NIFS-241 K. Ida, Y.Miura, T. Matsuda, K. Itoh and JFT-2M Group, *Observation of non Diffusive Term of Toroidal Momentum Transport in the JFT-2M Tokamak;* Aug. 1993

NIFS-242 O.J.W.F. Kardaun, S.-I. Itoh, K. Itoh and J.W.P.F. Kardaun, *Discriminant Analysis to Predict the Occurrence of ELMS in H-Mode Discharges;* Aug. 1993

NIFS-243 K. Itoh, S.-I. Itoh, A. Fukuyama, *Modelling of Transport Phenomena;* Sep. 1993

NIFS-244 J. Todoroki, *Averaged Resistive MHD Equations;* Sep. 1993

NIFS-245 M. Tanaka, *The Origin of Collisionless Dissipation in Magnetic Reconnection;* Sep. 1993

NIFS-246 M. Yagi, K. Itoh, S.-I. Itoh, A. Fukuyama and M. Azumi, *Current Diffusive Ballooning Mode in Seecond Stability Region of Tokamaks;* Sep. 1993

NIFS-247 T. Yamagishi, *Trapped Electron Instabilities due to Electron Temperature Gradient and Anomalous Transport;* Oct. 1993

NIFS-248 Y. Kondoh, *Attractors of Dissipative Structure in Three Disspative Fluids;* Oct. 1993

NIFS-249 S. Murakami, M. Okamoto, N. Nakajima, M. Ohnishi, H. Okada, *Monte Carlo Simulation Study of the ICRF Minority Heating in the Large Helical Device;* Oct. 1993

NIFS-250 A. Iiyoshi, H. Momota, O. Motojima, M. Okamoto, S. Sudo, Y. Tomita, S. Yamaguchi, M. Ohnishi, M. Onozuka, C. Uenosono, *Innovative Energy Production in Fusion Reactors*; Oct. 1993

NIFS-251 H. Momota, O. Motojima, M. Okamoto, S. Sudo, Y. Tomita, S. Yamaguchi, A. Iiyoshi, M. Onozuka, M. Ohnishi, C. Uenosono, *Characteristics of D-$^3$He Fueled FRC Reactor: ARTEMIS-L*, Nov. 1993

NIFS-252 Y. Tomita, L.Y. Shu, H. Momota, *Direct Energy Conversion System for D-$^3$He Fusion*, Nov. 1993

NIFS-253 S. Sudo, Y. Tomita, S. Yamaguchi, A. Iiyoshi, H. Momota, O. Motojima, M. Okamoto, M. Ohnishi, M. Onozuka, C. Uenosono, *Hydrogen Production in Fusion Reactors*, Nov. 1993

NIFS-254 S. Yamaguchi, A. Iiyoshi, O. Motojima, M. Okamoto, S. Sudo, M. Ohnishi, M. Onozuka, C. Uenosono, *Direct Energy Conversion of Radiation Energy in Fusion Reactor*, Nov. 1993

NIFS-255 S. Sudo, M. Kanno, H. Kaneko, S. Saka, T. Shirai, T. Baba, *Proposed High Speed Pellet Injection System "HIPEL" for Large Helical Device* Nov. 1993

NIFS-256 S. Yamada, H. Chikaraishi, S. Tanahashi, T. Mito, K. Takahata, N. Yanagi, M. Sakamoto, A. Nishimura, O. Motojima, J. Yamamoto, Y. Yonenaga, R. Watanabe, *Improvement of a High Current DC Power Supply System for Testing the Large Scaled Superconducting Cables and Magnets*; Nov. 1993

NIFS-257 S. Sasaki, Y. Uesugi, S. Takamura, H. Sanuki, K. Kadota, *Temporal Behavior of the Electron Density Profile During Limiter Biasing in the HYBTOK-II Tokamak*; Nov. 1993

NIFS-258 K. Yamazaki, H. Kaneko, S. Yamaguchi, K.Y. Watanabe, Y.Taniguchi, O.Motojima, LHD Group, *Design of Central Control System for Large Helical Device (LHD)*; Nov. 1993

NIFS-259 S. Yamada, T. Mito, A. Nishimura, K. Takahata, S. Satoh, J. Yamamoto, H. Yamamura, K. Masuda, S. Kashihara, K. Fukusada, E. Tada, *Reduction of Hydrocarbon Impurities in 200L/H Helium Liquefier-Refrigerator System*; Nov. 1993

NIFS-260 B.V.Kuteev, *Pellet Ablation in Large Helical Device*; Nov. 1993

NIFS-261 K. Yamazaki,
*Proposal of "MODULAR HELIOTRON': Advanced Modular Helical System Compatible with Closed Helical Divertor*; Nov. 1993

NIFS-262 V.D.Pustovitov,
*Some Theoretical Problems of Magnetic Diagnostics in Tokamaks and Stellarators*; Dec. 1993

NIFS-263 A. Fujisawa, H. Iguchi, Y. Hamada
*A Study of Non-Ideal Focus Properties of 30° Parallel Plate Energy Analyzers*; Dec. 1993

NIFS-264 K. Masai,
*Nonequilibria in Thermal Emission from Supernova Remnants*; Dec. 1993

NIFS-265 K. Masai, K. Nomoto,
*X-Ray Enhancement of SN 1987A Due to Interaction with its Ring-like Nebula*; Dec. 1993

NIFS-266 J. Uramoto
*A Research of Possibility for Negative Muon Production by a Low Energy Electron Beam Accompanying Ion Beam*; Dec. 1993

NIFS-267 H. Iguchi, K. Ida, H. Yamada, K. Itoh, S.-I. Itoh, K. Matsuoka, S. Okamura, H. Sanuki, I. Yamada, H. Takenaga, K. Uchino, K. Muraoka,
*The Effect of Magnetic Field Configuration on Particle Pinch Velocity in Compact Helical System (CHS)*; Jan. 1994

NIFS-268 T. Shikama, C. Namba, M. Kosuda, Y. Maeda,
*Development of High Time-Resolution Laser Flash Equipment for Thermal Diffusivity Measurements Usting Miniature-Size Specimens*; Jan. 1994

NIFS-269 T. Hayashi, T. Sato, P. Merkel, J. Nührenberg, U. Schwenn,
*Formation and 'Self-Healing' of Magnetic Islands in Finite-β Helias Equilibria*; Jan. 1994

NIFS-270 S. Murakami, M. Okamoto, N. Nakajima, T. Mutoh,
*Efficiencies of the ICRF Minority Heating in the CHS and LHD Plasmas*; Jan. 1994

NIFS-271 Y. Nejoh, H. Sanuki,
*Large Amplitude Langmuir and Ion-Acoustic Waves in a Relativistic Two-Fluid Plasma*; Feb. 1994

NIFS-272 A. Fujisawa, H. Iguchi, A. Taniike, M. Sasao, Y. Hamada,
*A 6MeV Heavy Ion Beam Probe for the Large Helical Device*;

Feb. 1994

NIFS-273 Y. Hamada, A. Nishizawa, Y. Kawasumi, K. Narihara, K. Sato, T. Seki, K. Toi, H. Iguchi, A. Fujisawa, K. Adachi, A. Ejiri, S. Hidekuma, S. Hirokura, K. Ida, J. Koong, K. Kawahata, M. Kojima, R. Kumazawa, H. Kuramoto, R. Liang, H. Sakakita, M. Sasao, K. N. Sato, T. Tsuzuki, J. Xu, I. Yamada, T. Watari, I. Negi,
*Measurement of Profiles of the Space Potential in JIPP T-IIU Tokamak Plasmas by Slow Poloidal and Fast Toroidal Sweeps of a Heavy Ion Beam*; Feb. 1994

NIFS-274 M. Tanaka,
*A Mechanism of Collisionless Magnetic Reconnection*; Mar. 1994

NIFS-275 A. Fukuyama, K. Itoh, S.-I. Itoh, M. Yagi and M. Azumi,
*Isotope Effect on Confinement in DT Plasmas*; Mar. 1994

NIFS-276 R.V. Reddy, K. Watanabe, T. Sato and T.H. Watanabe,
*Impulsive Alfven Coupling between the Magnetosphere and Ionosphere*; Apr.1994

NIFS-277 J. Uramoto,
*A Possibility of $\pi^-$ Meson Production by a Low Energy Electron Bunch and Positive Ion Bunch*; Apr. 1994

NIFS-278 K. Itoh, S.-I. Itoh, A. Fukuyama, M. Yagi and M. Azumi,
*Self-sustained Turbulence and L-mode Confinement in Toroidal Plasmas II*; Apr. 1994

NIFS-279 K. Yamazaki and K.Y.Watanabe,
*New Modular Heliotron System Compatible with Closed Helical Divertor and Good Plasma Confinement*; Apr. 1994

NIFS-280 S. Okamura, K. Matsuoka, K. Nishimura, K. Tsumori, R. Akiyama, S. Sakakibara, H. Yamada, S. Morita, T. Morisaki,. N. Nakajima, K. Tanaka, J. Xu, K. Ida, H. Iguchi, A. Lazaros, T. Ozaki, H. Arimoto, A. Ejiri, M. Fujiwara, H. Idei. O. Kaneko, K. Kawahata, T. Kawamoto, A. Komori, S. Kubo, O. Motojima, V.D. Pustovitov, C. Takahashi, K. Toi and I. Yamada,
*High-Beta Discharges with Neutral Beam Injection in CHS*,
Apr; 1994

NIFS-281 K. Kamada, H. Kinoshita and H. Takahashi,
*Anomalous Heat Evolution of Deuteron Implanted Al on Electron Bombardment ;* May 1994

NIFS-282 H. Takamaru, T. Sato, K. Watanabe and R. Horiuchi,
*Super Ion Acoustic Double Layer*; May 1994